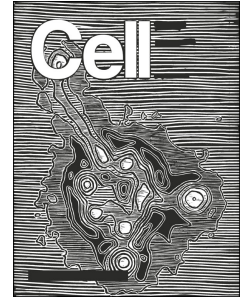


# Journal Pre-proof



Immune imprinting, breadth of variant recognition and germinal center response in human SARS-CoV-2 infection and vaccination

Katharina Röltgen, Sandra C.A. Nielsen, Oscar Silva, Sheren F. Younes, Maxim Zaslavsky, Cristina Costales, Fan Yang, Oliver F. Wirz, Daniel Solis, Ramona A. Hoh, Aihui Wang, Prabhu S. Arunachalam, Deana Colburg, Shuchun Zhao, Emily Haraguchi, Alexandra S. Lee, Mihir M. Shah, Monali Manohar, Iris Chang, Fei Gao, Vamsee Mallajosyula, Chunfeng Li, James Liu, Massa J. Shoura, Sayantani B. Sindhher, Ella Parsons, Naranjargal J. Dashdorj, Naranbaatar D. Dashdorj, Robert Monroe, Geidy E. Serrano, Thomas G. Beach, R. Sharon Chinthrajah, Gregory W. Charville, James L. Wilbur, Jacob N. Wohlstadter, Mark M. Davis, Bali Pulendran, Megan L. Troxell, George B. Sigal, Yasodha Natkunam, Benjamin A. Pinsky, Kari C. Nadeau, Scott D. Boyd

PII: S0092-8674(22)00076-9

DOI: <https://doi.org/10.1016/j.cell.2022.01.018>

Reference: CELL 12350

To appear in: *Cell*

Received Date: 10 November 2021

Revised Date: 3 January 2022

Accepted Date: 20 January 2022

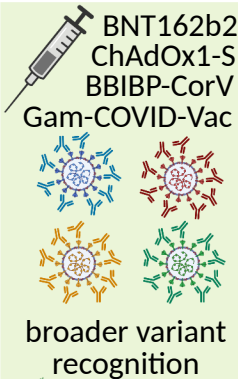
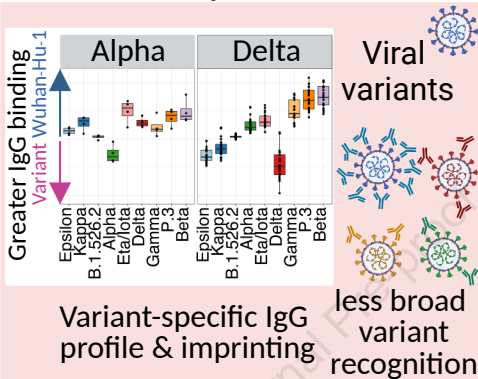
Please cite this article as: Röltgen, K., Nielsen, S.C.A., Silva, O., Younes, S.F., Maxim Zaslavsky, Costales, C., Yang, F., Wirz, O.F., Solis, D., Hoh, R.A., Wang, A., Arunachalam, P.S., Colburg, D., Zhao, S., Haraguchi, E., Lee, A.S., Shah, M.M., Manohar, M., Chang, I., Gao, F., Mallajosyula, V., Li, C., Liu, J., Shoura, M.J., Sindhher, S.B., Parsons, E., Dashdorj, N.J., Dashdorj, N.D., Monroe, R., Serrano, G.E., Beach, T.G., Chinthrajah, R.S., Charville, G.W., Wilbur, J.L., Wohlstadter, J.N., Davis, M.M., Pulendran, B., Troxell, M.L., Sigal, G.B., Natkunam, Y., Pinsky, B.A., Nadeau, K.C., Boyd, S.D., Immune imprinting, breadth of variant recognition and germinal center response in human SARS-CoV-2 infection and vaccination, *Cell* (2022), doi: <https://doi.org/10.1016/j.cell.2022.01.018>.

This is a PDF file of an article that has undergone enhancements after acceptance, such as the addition of a cover page and metadata, and formatting for readability, but it is not yet the definitive version of

record. This version will undergo additional copyediting, typesetting and review before it is published in its final form, but we are providing this version to give early visibility of the article. Please note that, during the production process, errors may be discovered which could affect the content, and all legal disclaimers that apply to the journal pertain.

© 2022 Published by Elsevier Inc.

Anti-CoV-2 plasma IgG

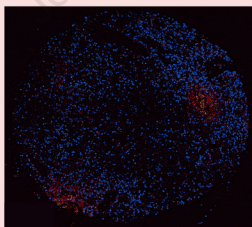


GC response

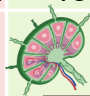
Severe COVID-19



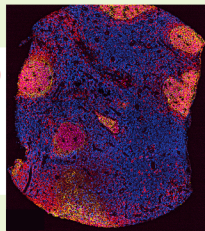
Post-mortem lymph node (LN)



Impaired germinal centers (GCs)



Post-mRNA vaccine LN



Intact GCs

CD20  
CD3  
BCL6  
CD21

1 Immune imprinting, breadth of variant recognition and germinal center response in  
2 human SARS-CoV-2 infection and vaccination

3  
4 Katharina Röltgen<sup>1†</sup>, Sandra C. A. Nielsen<sup>1†</sup>, Oscar Silva<sup>1†</sup>, Sheren F. Younes<sup>1†</sup>, Maxim  
5 Zaslavsky<sup>1</sup>, Cristina Costales<sup>1</sup>, Fan Yang<sup>1</sup>, Oliver F. Wirz<sup>1</sup>, Daniel Solis<sup>1</sup>, Ramona A. Hoh<sup>1</sup>, Aihui  
6 Wang<sup>1</sup>, Prabhu S. Arunachalam<sup>2</sup>, Deana Colburg<sup>1</sup>, Shuchun Zhao<sup>1</sup>, Emily Haraguchi<sup>1</sup>, Alexandra  
7 S. Lee<sup>3</sup>, Mihir M. Shah<sup>3</sup>, Monali Manohar<sup>3</sup>, Iris Chang<sup>3</sup>, Fei Gao<sup>2</sup>, Vamsee Mallajosyula<sup>2</sup>,  
8 Chunfeng Li<sup>2</sup>, James Liu<sup>4</sup>, Massa J. Shoura<sup>1</sup>, Sayantani B. Sindher<sup>3</sup>, Ella Parsons<sup>3</sup>, Naranjargal J.  
9 Dashdorj<sup>5,6</sup>, Naranbaatar D. Dashdorj<sup>5</sup>, Robert Monroe<sup>7</sup>, Geidy E. Serrano<sup>8</sup>, Thomas G. Beach<sup>8</sup>,  
10 R. Sharon Chinthrajah<sup>3,9</sup>, Gregory W. Charville<sup>1</sup>, James L. Wilbur<sup>10</sup>, Jacob N. Wohlstadter<sup>10</sup>, Mark  
11 M. Davis<sup>2,11,12</sup>, Bali Pulendran<sup>1,2,11</sup>, Megan L. Troxell<sup>1</sup>, George B. Sigal<sup>10</sup>, Yasodha Natkunam<sup>1</sup>,  
12 Benjamin A. Pinsky<sup>1,13</sup>, Kari C. Nadeau<sup>3,9‡</sup>, Scott D. Boyd<sup>1,3‡\*</sup>

13  
14 \*Lead contact: Scott D. Boyd, email: [publications\\_scott\\_boyd@stanford.edu](mailto:publications_scott_boyd@stanford.edu)

15  
16 <sup>1</sup>Department of Pathology, Stanford University, Stanford, CA, USA

17 <sup>2</sup>Institute for Immunity, Transplantation and Infection, Stanford University, Stanford, CA, USA

18 <sup>3</sup>Sean N. Parker Center for Allergy & Asthma Research, Stanford University, Stanford, CA, USA

19 <sup>4</sup>Stanford Health Library, Stanford, CA, USA

20 <sup>5</sup>Onom Foundation, Ulaanbaatar 17013, Mongolia

21 <sup>6</sup>Liver Center, Ulaanbaatar 14230, Mongolia

22 <sup>7</sup>Advanced Cell Diagnostics, Newark, CA, USA

23 <sup>8</sup>Banner Sun Health Research Institute, Sun City, AZ, USA

24 <sup>9</sup>Department of Medicine, Division of Pulmonary, Allergy, and Critical Care Medicine, Stanford  
25 University, Stanford, CA, USA

26 <sup>10</sup>Meso Scale Diagnostics LLC, Rockville, Maryland, USA

27 <sup>11</sup>Department of Microbiology and Immunology, Stanford University, Stanford, CA, USA

28 <sup>12</sup>Howard Hughes Medical Institute, Stanford University, Stanford, CA, USA

29 <sup>13</sup>Department of Medicine, Division of Infectious Diseases and Geographic Medicine, Stanford  
30 University, Stanford, CA USA

31

32 †these authors contributed equally to this work

33 ‡these authors contributed equally to this work

## 34 **Summary**

35 During the SARS-CoV-2 pandemic, novel and traditional vaccine strategies have been deployed  
36 globally. We investigated whether antibodies stimulated by mRNA vaccination (BNT162b2),  
37 including 3<sup>rd</sup> dose boosting, differ from those generated by infection or adenoviral (ChAdOx1-S  
38 and Gam-COVID-Vac) or inactivated viral (BBIBP-CorV) vaccines. We analyzed human lymph  
39 nodes after infection or mRNA vaccination for correlates of serological differences. Antibody  
40 breadth against viral variants is less after infection compared to all vaccines evaluated, but  
41 improves over several months. Viral variant infection elicits variant-specific antibodies, but prior  
42 mRNA vaccination imprints serological responses toward Wuhan-Hu-1 rather than variant  
43 antigens. In contrast to disrupted germinal centers (GCs) in lymph nodes during infection,  
44 mRNA vaccination stimulates robust GCs containing vaccine mRNA and spike antigen up to 8  
45 weeks post-vaccination in some cases. SARS-CoV-2 antibody specificity, breadth and  
46 maturation are affected by imprinting from exposure history, and distinct histological and  
47 antigenic contexts in infection compared to vaccination.

48

49

50

## 51 **Keywords**

52 COVID-19; BioNTech-Pfizer; BNT162b2; Moderna; mRNA-1273; AstraZeneca; ChAdOx1-S;  
53 Sputnik V; Gam-COVID-Vac; Sinopharm; BBIBP-CorV; mRNA vaccine; serology;  
54 electrochemiluminescence; SARS-CoV-2; imprinting; variants of concern; Delta variant; endemic  
55 coronaviruses; antibodies; germinal center; lymph node biopsy; autopsy

56

## 57 **Introduction**

58 The urgent need for countermeasures against the coronavirus disease 2019 (COVID-19) pandemic  
59 has spurred rapid development of SARS-CoV-2 vaccines of diverse formulations. mRNA vaccines  
60 BNT162b2 (BioNTech-Pfizer) and mRNA-1273 (Moderna/NIAID) have demonstrated high  
61 efficacy and safety in clinical trials for COVID-19 prevention (Baden et al., 2021; Polack et al.,  
62 2020; Walsh et al., 2020). Additional COVID-19 vaccines including adenoviral vectored vaccines  
63 ChAdOx1-S (AstraZeneca) (Voysey et al., 2021), Ad26.COV2.S (Johnson & Johnson) (Sadoff et  
64 al., 2021), and Gam-COVID-Vac (Sputnik V), and inactivated viral vaccines such as BBIBP-CorV  
65 (Sinopharm), also have reported efficacy. Correlates of vaccine-elicited protection from COVID-  
66 19 are the titers of neutralizing antibodies to SARS-CoV-2, and the concentration of antibodies  
67 binding to spike or receptor binding domain (RBD) (Earle et al., 2021; Gilbert et al., 2022; Khoury  
68 et al., 2021; Röltgen and Boyd, 2021). Most neutralizing antibodies target the RBD and prevent  
69 binding to angiotensin-converting enzyme 2 (ACE2) receptor (Greaney et al., 2021a; Yuan et al.,  
70 2021). Current SARS-CoV-2 vaccines all contain or induce expression of antigens similar to those  
71 of the early Wuhan-Hu-1 viral isolate, but differ in elicited binding and neutralizing antibody  
72 responses, with higher responses from mRNA vaccines compared to adenovirus-vectored or  
73 inactivated virus vaccines (Dashdorj et al., 2021a, 2021b). It remains to be determined precisely  
74 how the immune system responds to mRNA and other vaccine platforms compared to SARS-CoV-  
75 2 infection. Data from RBD variant antigen yeast display and pseudotyped virus neutralization  
76 show that RBD epitope targeting by polyclonal serum antibodies is narrower in infected patients  
77 compared to mRNA-1273 vaccinees (Greaney et al., 2021b).

78 Several SARS-CoV-2 variants of concern with mutations in the spike gene have emerged and  
79 spread globally, with differing abilities to evade neutralizing antibody responses elicited by

80 Wuhan-Hu-1 infection or vaccination. The most immune-evasive variants, including the recent  
81 Omicron variant, have alterations in epitopes containing amino acid E484 (Garcia-Beltran et al.,  
82 2021; Greaney et al., 2021a; Hoffmann et al., 2021). The appearance of virus variants, waning  
83 antibody levels after infection or vaccination (Falsey et al., 2021; Levin et al., 2021), and  
84 breakthrough infections in previously immunized individuals (Keehner et al., 2021) indicate that  
85 periodic vaccine boosting of immunity to SARS-CoV-2 is warranted. Third doses of mRNA-1273  
86 (Chu et al., 2021) and BNT162b2 (Falsey et al., 2021) administered several months after the  
87 second dose prompt an increase in neutralizing antibodies greater than the peak following initial  
88 vaccination doses. mRNA-1273 vaccination followed by mRNA booster vaccines expressing Beta  
89 spike gives higher neutralizing titers to Wuhan-Hu-1-like SARS-CoV-2 compared to the Beta  
90 variant (Choi et al., 2021; Wu et al., 2021), suggesting that some degree of immune imprinting, or  
91 preferential responses to the viral variants initially encountered by the immune system, may affect  
92 the development of antibodies against new viral variants (Wheatley et al., 2021).

93  
94 Germinal center (GC) responses in human lymphoid tissues enable antibody affinity maturation  
95 and durable serological and memory B cell responses, although extrafollicular B cell responses are  
96 also reported (Elsner and Shlomchik, 2020; Lam et al., 2020; Woodruff et al., 2020). The degree  
97 to which SARS-CoV-2 infections or different vaccines stimulate GC responses and differ in factors  
98 such as the quantity, persistence and localization of antigen in lymph nodes (LNs) and other  
99 lymphoid tissues are important open questions. Approaches such as fine-needle aspiration (FNA)  
100 are being increasingly used to study LN-derived cells from healthy human subjects (Havenar-  
101 Daughton et al., 2020; Lederer et al., 2021; Turner et al., 2021). Disrupted LN GCs have been  
102 reported in autopsies of deceased COVID-19 patients (Haslbauer et al., 2021; Kaneko et al., 2020),

103 while elevated frequencies of GC B cells are seen after mRNA vaccination in healthy individuals  
104 (Turner et al., 2021), and lower GC B cell frequencies after mRNA vaccination of  
105 immunocompromised individuals (Lederer et al., 2021). To date, no direct comparison of LN GC  
106 histology and cellular composition, combined with measurement of viral or vaccine antigen  
107 quantity, persistence and distribution in draining LN sites of COVID-19 patients and vaccinees  
108 has been reported.

109  
110 Here, we compare antibody responses in BNT162b2 mRNA vaccine recipients following 1<sup>st</sup>, 2<sup>nd</sup>  
111 and 3<sup>rd</sup> vaccine doses, to antibody responses of COVID-19 patients. We find differences in the  
112 magnitude, isotype profiles, SARS-CoV-2 spike domain specificity and breadth of binding  
113 antibody responses to a panel of nine viral variants in addition to Wuhan-Hu-1. Anti-RBD IgG  
114 binding to SARS-CoV-2 variants of concern and interest in recipients of four different vaccines  
115 (BNT162b2, ChAdOx1-S, Gam-COVID-Vac, and BBIBP-CorV) and in COVID-19 patients,  
116 shows greater binding breadth for viral variant RBDs following all vaccines compared to Wuhan-  
117 Hu-1 infection. We quantify a strong imprinting effect of prior vaccination with Wuhan-Hu-1  
118 spike antigen on antibody specificities following breakthrough infection with viral variants.  
119 Histological analysis of draining LN shows marked impairment of GCs in severe COVID-19  
120 compared to mRNA vaccination, higher quantities and persistence of spike antigen accumulated  
121 in the GCs of mRNA vaccinees, and detectable vaccine RNA in GCs for up to two months post-  
122 2<sup>nd</sup> dose.

123

124 **Results**

125 *Magnitude and waning of anti-SARS-CoV-2 IgG following BNT162b2 vaccination, and*  
126 *response to 3<sup>rd</sup> dose boost*

127 We measured anti-SARS-CoV-2 antibodies for nucleocapsid (N), full spike and RBD in Stanford  
128 BNT162b2 study participant plasma samples using multiplexed electrochemiluminescence (ECL)  
129 assays (Meso Scale Discovery, MSD), in WHO Binding Antibody Units (BAU). The first and  
130 second vaccine doses were at day 0 and day 21, with third dose boosting at approximately 9  
131 months. Plasma samples were collected in a time course up to seven months after the first dose,  
132 and up to one month after the third dose. Four of the 59 vaccine recipients had a history of SARS-  
133 CoV-2 reverse-transcription quantitative polymerase chain reaction (RT-qPCR)-confirmed  
134 infection (CoV-2+) prior to vaccination. IgG for spike protein and RBD in vaccinees reached their  
135 initial peak at day 28 after the first dose (Figures 1A and 1B). IgG binding to spike and RBD was  
136 highly correlated with SARS-CoV-2 neutralization titers (Arunachalam et al., 2021) (Figure 1C).  
137 By 9 months, spike-specific IgG had decreased approximately 20-fold from the maximum, but the  
138 3<sup>rd</sup> dose boost raised IgG concentrations above the prior peak within one week. IgG specific for N  
139 protein, which is not encoded in the vaccine, was negative throughout the study in 54 of the  
140 previously uninfected vaccinees, but one participant seroconverted for anti-N IgG between day 90  
141 and 210 after the prime, indicating a breakthrough infection (Figure 1A). CoV-2+ vaccinees had  
142 accelerated RBD and spike IgG responses after the first dose, and detectable anti-N IgG unaffected  
143 by vaccination (Figure S1A).

144  
145 BNT162b2 recipients had weak IgM and IgA responses to spike and RBD compared to their IgG  
146 responses. Robust IgG responses were seen in all age groups (Figure 1B; Figures S1A - S1C).  
147 Convalescent COVID-19 patients and BNT162b2 vaccinees had similar low saliva IgG

148 concentrations for spike and RBD, several orders of magnitude lower than those detected in plasma  
149 (Figure S1D). As in plasma, saliva IgG peaked at one week after 3<sup>rd</sup> dose boosting, at higher values  
150 than the peak after the 2<sup>nd</sup> dose (Figure S1D). Reported side-effects after vaccination showed no  
151 relationship to plasma IgG responses (Figures S2A and S2B).

152

153 ***BNT162b2 vaccination and Wuhan-Hu-1 SARS-CoV-2 infection stimulate distinct antibody***  
154 ***isotypes and endemic coronavirus antibody responses***

155 Severe COVID-19 stimulates higher SARS-CoV-2-specific antibody titers than asymptomatic  
156 infection or mild illness (Long et al., 2020; Röltgen et al., 2020). We compared antibody isotype  
157 concentrations specific for spike and RBD in COVID-19 patients (Stanford cohort 1 of this study)  
158 from the initial months of the pandemic (Röltgen et al., 2020), to the responses of the Stanford  
159 BNT162b2 vaccinees (Figures 2A and 2B). Patients were classified as outpatients; admitted  
160 patients not requiring care in the intensive care unit (ICU); ICU patients; and those who died from  
161 their illness. Stanford BNT162b2 vaccinee RBD and spike IgG concentrations were comparable  
162 to those of severely ill patients, and higher than those of mildly or moderately ill patients for anti-  
163 RBD antibodies at day 42 (Figures 2A and 2B). The BNT162b2 vaccine induced a highly IgG-  
164 polarized serological response with minimal IgM and IgA binding spike and RBD (Figures 2A  
165 and 2B). Principal component analysis (PCA) showed clustered and homogeneous SARS-CoV-2  
166 spike and spike domain-specific serological responses in BNT162b2 vaccinees compared to  
167 infected patients, as quantified by smaller distances for vaccinated participants from the group  
168 centroid (Figures 2C and 2D).

169 SARS-CoV-2 vaccinees and COVID-19 patients showed boosting of SARS-CoV-1 spike  
170 antibodies, but infected patients showed greater boosting of spike IgG and IgA for endemic human

171 betacoronaviruses OC43 and HKU1 (Figures S3A and S3B). The 3<sup>rd</sup> BNT162b2 vaccine dose  
172 further increased vaccinee titers to SARS-CoV-1, OC43, and HKU1 (Figure S3C). Antibodies to  
173 the spike antigens of the endemic human alphacoronaviruses NL63 and 229E were not boosted  
174 (Figure S3).

175

176 ***Greater breadth of IgG binding to viral variants following BNT162b2 vaccination compared to***  
177 ***infection with Wuhan-Hu-1 SARS-CoV-2***

178 Immune-evasive SARS-CoV-2 variants have spread globally (Harvey et al., 2021; Plante et al.,  
179 2021; Röltgen and Boyd, 2021). We compared plasma IgG responses to the RBDs of nine different  
180 SARS-CoV-2 variants of concern and interest in BNT162b2 vaccinees and COVID-19 patients,  
181 using multiplexed MSD ECL assays. For RBD antigens from Epsilon, Kappa, B.1.526.2,  
182 B.1.214.2, Alpha, Eta/Iota, Gamma, P.3, and Beta variants, both vaccinee and infected patient IgG  
183 showed the greatest decrease in binding to Beta, Gamma, and P.3 variants relative to Wuhan-Hu-  
184 1 (Figure 3A). To quantify the differences in variant RBD binding by vaccinee and patient plasma  
185 IgG we calculated the ratios of anti-RBD IgG concentrations for Wuhan-Hu-1 compared to viral  
186 variants, with higher ratios indicating greater binding of Wuhan-Hu-1 RBD compared to variant  
187 RBD (Figure 3B). COVID-19 patients showed a greater IgG binding bias for Wuhan-Hu-1 RBD  
188 compared to variant RBDs in the initial weeks post-onset of symptoms; in contrast, BNT162b2  
189 vaccinee IgG had relatively greater breadth of binding to variant RBDs and less preference for  
190 Wuhan-Hu-1 RBD. Over time, infected patient plasma samples showed improvement in variant  
191 RBD binding relative to Wuhan-Hu-1 RBD, suggesting evolution of the antibody response through  
192 at least 7 weeks post-onset of symptoms (Figure 3). BNT162b2 vaccinee IgG Wuhan-Hu-1 to  
193 variant RBD binding ratios did not change from day 21 onward. The greater breadth of variant

194 RBD binding (including the Delta variant) by vaccinee IgG compared to COVID-19 patient IgG  
195 was seen in a second, independent validation cohort (Stanford cohort 2) of predominantly mildly  
196 ill COVID-19 patients. Greater Wuhan-Hu-1 to variant RBD IgG binding ratios were found in  
197 week 2 to 3, month 1, month 3, and month 7 in infected patients compared to vaccinees (Figures  
198 S4A and S4B), with improvement in variant recognition over time in the infected patients. Notably,  
199 the increased breadth of vaccinee IgG compared to COVID-19 patient IgG binding to viral variant  
200 antigens was greatest for RBD, the main target of neutralizing antibodies, and was decreased or  
201 not detected when whole spike antigens were tested (Figure S4C). Functional blocking of ACE2  
202 binding to RBD was concordant with the RBD-specific IgG concentrations measured in these  
203 populations (Figures S4A and S4D).

204

205 ***Improved IgG binding to viral variants is consistent across four COVID-19 vaccines***  
206 ***(BNT162b2, ChAdOx1-S, Gam-COVID-Vac and BBIBP-CorV) compared to infection***

207 Several COVID-19 vaccines, including mRNA, viral vector-based, and inactivated virus vaccines,  
208 have been approved for use internationally. Varying efficacy and antibody responses from the  
209 vaccines have been reported (Baden et al., 2021; Dashdorj et al., 2021a, 2021b; Polack et al., 2020;  
210 Sadoff et al., 2021; Voysey et al., 2021). We compared IgG responses in Stanford COVID-19  
211 cohort 2 patients and BNT162b2 vaccinees to those of participants in a Mongolian observational  
212 study deploying four different COVID-19 vaccines: the mRNA vaccine BNT162b2; adenoviral  
213 vectored vaccines ChAdOx1-S (AstraZeneca) and Gam-COVID-Vac (Sputnik V); and an alum-  
214 adjuvanted, inactivated viral vaccine BBIBP-CorV (Sinopharm). RBD-specific IgG  
215 concentrations for Wuhan-Hu-1 and all viral variants measured (Epsilon, Kappa, B.1.526.2, Delta,  
216 Alpha, Eta/Iota, Gamma, P.3, and Beta) differed greatly between vaccine groups, with BNT162b2

217 eliciting the highest antibody levels, followed by AstraZeneca, Sputnik V, and Sinopharm  
218 vaccination (Figure 4A). IgG concentration differences between vaccines were significant for most  
219 viral variant RBDs. Stanford BNT162b2 vaccinees compared to Mongolian BNT162b2 vaccinees  
220 had higher IgG concentrations at early time points, likely due to differences in timing of sample  
221 collection (Stanford day 28 and day 90; Mongolian participants variable time points before 1-  
222 month and 3-months) (Figure 4A). Despite the different vaccine compositions and magnitudes of  
223 antibody responses, all four vaccines elicited IgG with relatively greater breadth of viral variant  
224 RBD binding compared to that of infected patients (Figure 4B).

225

226 ***Variant-specific serological responses following Alpha and Delta SARS-CoV-2 infection, and***  
227 ***immune imprinting after vaccination***

228 Immune imprinting, a phenomenon in which primary exposure to an antigen forms epitope-  
229 specific B cell memory and affects future B cell and antibody responses against variant epitopes,  
230 has been studied in influenza infection and vaccination. COVID-19 patients and BNT162b2  
231 vaccinees who were only exposed to Wuhan-Hu-1 antigens in this study exhibit a consistent  
232 hierarchy in IgG binding concentrations to the different SARS-CoV-2 variant RBDs relative to the  
233 Wuhan-Hu-1 RBD, decreasing from Epsilon, Kappa, B.1.526.2, Delta, Alpha, Eta/Iota, Gamma,  
234 P.3, to Beta (Figure S5A). To test for imprinting of the serological response to variant RBDs, we  
235 first analyzed the ratios of Wuhan-Hu-1 to variant RBD IgG concentrations in COVID-19 patients  
236 who were infected with Alpha or Delta variants, confirmed by allele-specific RT-qPCR testing or  
237 viral sequencing. IgG from Alpha or Delta variant-infected patients with no history of COVID-19  
238 vaccination or prior SARS-CoV-2 infection preferentially bound Alpha and Delta variant RBDs,  
239 respectively, compared to Wuhan-Hu-1 RBD (Figure 5A, upper panels). Delta infection also

240 elicited higher IgG concentrations to other variant RBDs containing L452R such as Epsilon and  
241 Kappa, compared to Wuhan-Hu-1 (Figure 5A, upper right). PCA of variant RBD-specific IgG  
242 responses in vaccinees and variant-infected patients (Figure S5B) highlights the distinct  
243 serological responses elicited by infection with the variant viruses. To test whether prior exposure  
244 to one SARS-CoV-2 RBD variant causes imprinting of humoral immunity, we analyzed plasma  
245 from individuals vaccinated with Wuhan-Hu-1-like antigens and subsequently infected with Alpha  
246 or Delta variants (Figure 5A, lower panels). Despite breakthrough infection with Alpha or Delta  
247 viral variants, the vaccinated individuals showed patterns of IgG binding to viral variant RBDs  
248 similar to those of individuals exposed to only Wuhan-Hu-1. We quantified the degree of  
249 imprinting of IgG specificity by log-transforming the ratios of IgG binding to pairs of antigens (for  
250 example, Wuhan-Hu-1 RBD compared to Delta RBD) for individual samples, then rescaling to  
251 range from -100% to +100% corresponding to the maximal preference for each antigen observed  
252 in other plasma specimens, including those from individuals exposed only to a single antigen  
253 variant (Figure 5B).

254

255 ***LN GC impairment in severe SARS-CoV-2 infection but robust development following SARS-***  
256 ***CoV-2 mRNA vaccination***

257 The differences in viral variant RBD IgG binding between SARS-CoV-2 infected patients and  
258 recipients of the four COVID-19 vaccines suggest that the organization of the humoral immune  
259 responses in secondary lymphoid tissues may differ between infection and vaccination, potentially  
260 due to direct effects of the viral infection, differences in innate immune stimuli between  
261 vaccination and infection, or the quantity or localization of viral antigens, among other  
262 possibilities. Previous studies have revealed a loss of GCs and a reduction in BCL6<sup>+</sup> GC B cells

263 in severe acute SARS-CoV-2 infection, raising the possibility that humoral responses may be  
264 altered or subverted by the virus (Kaneko et al., 2020). It is unclear whether draining LN immune  
265 responses to SARS-CoV-2 infection in the lungs differ from those elicited in axillary LNs  
266 following deltoid intramuscular mRNA vaccination. To compare GC architecture in response to  
267 SARS-CoV-2 infection and vaccination, we obtained peribronchial LN tissues from six COVID-  
268 19 patients and three control autopsy cases as well as axillary LN core needle biopsies of seven  
269 individuals vaccinated with mRNA-1273 or BNT162b2. Importantly, core needle biopsy sample  
270 tissue volumes were suitable for assessment of LN histoarchitecture. Vaccinee axillary LN  
271 biopsies were from the ipsilateral (same-side) arm vaccinated. Controls were thoracic LNs from  
272 individuals who succumbed to pre-pandemic non-COVID-19 pneumonias, and contain GCs likely  
273 due to ongoing adaptive immune responses elicited by other antigens. LN histology for COVID-  
274 19 patients and vaccinees was evaluated with 4-color co-detection by indexing (CODEX)  
275 immunofluorescence analysis for CD20, CD3, BCL6 and CD21, which are markers of B cells, T  
276 cells, GC B cells (or T follicular helper (Tfh) cells) and follicular dendritic cells, respectively  
277 (Figure 6A, Figure S6A), as well as by single-color immunohistochemical stains for these markers  
278 and the Tfh cell marker PD-1 (Figure 6B). GCs were poorly formed in the severely ill COVID-19  
279 patient peribronchial LNs compared to the axillary LNs of vaccinees, with disrupted CD21+  
280 follicular dendritic cell networks and decreased BCL6<sup>+</sup> cells (including GC B cells and Tfh cells)  
281 and PD-1<sup>+</sup> cells (consistent with Tfh cells) within GCs (Figures 6A - 6E). Disruption of CD21+  
282 follicular dendritic cell networks was seen in both primary and secondary follicles in LNs from  
283 COVID-19 patients (Figure S6B). mRNA vaccination was associated with follicular hyperplasia  
284 with fully developed GC architecture, including robust induction of GC B cells, Tfh cells and  
285 extensive follicular dendritic cell networks (Figures 6A and 6B).

286

287 ***Prolonged detection of vaccine mRNA in LN GCs, and spike antigen in LN GCs and blood***  
288 ***following SARS-CoV-2 mRNA vaccination***

289 The biodistribution, quantity and persistence of vaccine mRNA and spike antigen after  
290 vaccination, and viral antigens after SARS-CoV-2 infection, are incompletely understood but are  
291 likely to be major determinants of immune responses. We performed *in situ* hybridization with  
292 control and SARS-CoV-2 vaccine mRNA-specific RNAScope probes in the core needle biopsies  
293 of the ipsilateral axillary LNs that were collected 7-60 days after 2<sup>nd</sup> dose of mRNA-1273 or  
294 BNT162b2 vaccination, and detected vaccine mRNA collected in the GCs of LNs on day 7, 16,  
295 and 37 post vaccination, with lower but still appreciable specific signal at day 60 (Figures 7A -  
296 7E). Only rare foci of vaccine mRNA were seen outside of GCs. Axillary LN core needle biopsies  
297 of non-vaccinees (n = 3) and COVID-19 patient specimens were negative for vaccine probe  
298 hybridization. Immunohistochemical staining for spike antigen in mRNA vaccinated patient LNs  
299 varied between individuals, but showed abundant spike protein in GCs 16 days post-2<sup>nd</sup> dose, with  
300 spike antigen still present as late as 60 days post-2<sup>nd</sup> dose. Spike antigen localized in a reticular  
301 pattern around the GC cells, similar to staining for follicular dendritic cell processes (Figure 7B).  
302 COVID-19 patient LNs showed lower quantities of spike antigen, but a rare GC had positive  
303 staining (Figure 7F). Immunohistochemical staining for N antigen in peribronchial LN secondary  
304 and primary follicles of COVID-19 patients (Figures 7F - 7I) was positive in 5 of the 7 patients,  
305 with a mean percentage of nucleocapsid-positive follicles of more than 25%.

306

307 Spike protein was detected in the plasma of 96% of the vaccinees at days 1-2 (median spike  
308 concentration of 47 pg/mL) and in 63% at day 7 (median spike concentration of 1.7 pg/mL) after

309 the prime vaccine dose. In contrast, spike antigen detection after the vaccine boost on day 21 was  
310 reduced, with half of the study participants being positive on day 1-2 (median spike concentration  
311 of 1.2 pg/mL) and only one individual on day 7 post-boost (Figure 7J). We suspected that high  
312 concentrations of spike-specific antibodies developed by vaccinees within the first 2 to 3 weeks  
313 after the prime vaccine dose could impede detection of spike antigen by competing for spike  
314 binding sites with the anti-spike reagent antibodies in the antigen assay. To test this hypothesis,  
315 we added different concentrations of recombinant spike protein to spike-negative vaccinee plasma  
316 samples collected on day 0 (n = 3) and day 28 (n = 3) after the prime vaccination. While the  
317 recombinant spike protein could readily be detected in day 0 plasma samples, only high  
318 concentrations of the antigen led to a positive signal when mixed with the day 28 samples (Figure  
319 7K). We then mixed a spike-positive plasma sample collected one day after vaccination with spike-  
320 negative plasma samples collected on days 0, 21, 22-23, and 28 (n = 4 each). Spike antigen  
321 detection levels were high in the mix of day 1 and day 0 samples, decreased in the mix of day 1  
322 and day 21, and day 1 and day 22-23 samples, and below the cutoff for positive in the mix of day  
323 1 and day 28 samples (Figure 7L). Together our results are consistent with spike-specific  
324 antibodies blocking detection of the antigen in antigen capture-based assays.

325

## 326 **Discussion**

327 One of the positive developments amid the global calamity of the SARS-CoV-2 pandemic has  
328 been the rapid design, production and deployment of a variety of vaccines, including remarkably  
329 effective mRNA vaccines encoding the viral spike (Baden et al., 2021; Polack et al., 2020). We  
330 find that BNT162b2 vaccination produces IgG responses to spike and RBD at concentrations as  
331 high as those of severely ill COVID-19 patients and follows a similar time course. Unlike infection,

332 which stimulates robust but short-lived IgM and IgA responses, vaccination shows a pronounced  
333 bias for IgG production even at early time points. These responses were similar across the adult  
334 age range in our study. The relative absence of IgM and IgA responses suggests a potent effect of  
335 the vaccine formulation in driving early and extensive IgG class-switching, potentially as a result  
336 of the reported T helper type 1-polarized CD4<sup>+</sup> T cell responses stimulated by vaccine components  
337 (Lederer et al., 2020; Lindgren et al., 2017; Pardi et al., 2018). Our data demonstrate that vaccinee  
338 plasma and saliva spike and RBD-specific IgG concentrations decrease from their peak values by  
339 approximately 20-fold by 9 months after primary vaccination, but quickly exceed prior peak  
340 concentrations in 7 to 8 days after boosting with a 3<sup>rd</sup> vaccine dose.

341  
342 Correlates of immunological protection from SARS-CoV-2 infection following vaccination or  
343 prior infection are still under investigation. Analysis of Moderna mRNA-1273 and AstraZeneca  
344 ChAdOx1-S responses highlights the overall similarity of correlate of protection results for spike-  
345 binding antibody and neutralizing antibody assays (Feng et al., 2021; Gilbert et al., 2022). We  
346 compared spike or RBD-binding antibody responses to Wuhan-Hu-1 SARS-CoV-2 neutralization  
347 data in BNT162b2 vaccinees and confirmed the high correlation of these assay results, supporting  
348 the interpretation that sensitive, precise and validated commercial multiplexed antigen-binding  
349 assays with a wide dynamic range, such as the MSD ECL assays in this study, will be valuable in  
350 providing standardized correlates of protection data for vaccines as the pandemic continues.  
351 Particularly in the context of viral variants, it will be important to determine whether predictions  
352 of vulnerability to infection or severe disease can be improved by adding data from other  
353 immunological assays, including T cell measurements.

354

355 Differences in B cell responses to SARS-CoV-2 infection and vaccination may be reflected in the  
356 binding breadth of antibodies to different SARS-CoV-2 variants. We find that plasma of  
357 individuals who received prime/boost BNT162b2 vaccination, as well as individuals who received  
358 adenoviral vectored (ChAdOx1-S or Gam-COVID-Vac) or inactivated virus (BBIBP-CorV)  
359 COVID-19 vaccines show consistent patterns of binding to variant RBDs with modest decreases  
360 compared to Wuhan-Hu-1 RBD binding. In contrast, COVID-19 patients produce antibody  
361 responses with significantly greater Wuhan-Hu-1 RBD binding preference and lower breadth of  
362 variant RBD binding. These differences between vaccinee and COVID-19 patient IgG variant  
363 antigen binding were greatest for the RBD, the target of most neutralizing antibodies, and were  
364 diminished when full spike antigen with its greater number of non-neutralizing epitopes was tested.  
365 These results, covering many clinically relevant viral variant antigens and several vaccine  
366 modalities, are consistent with findings for RBD binding IgG in mRNA-1273 vaccinees compared  
367 to infected patients (Greaney et al., 2021b). Notably, COVID-19 patients with Alpha or Delta  
368 variant infections display characteristic serological profiles specific to the RBD of the infecting  
369 variant, indicating that SARS-CoV-2 variant serotyping may be useful for epidemiological studies  
370 of populations to determine exposure to circulating SARS-CoV-2 variants. Both vaccinees and  
371 COVID-19 patients exposed to Wuhan-Hu-1 antigens show the greatest decreases in antibody  
372 binding to RBD variants harboring E484 alterations, including Beta and Gamma. Although  
373 susceptibility to infection by viral variants is common to both vaccinated and convalescent  
374 populations, particularly as antibody titers decrease over time (Israel et al., 2021; Levin et al.,  
375 2021), our findings lead to the prediction that antibodies derived from infection may provide  
376 somewhat decreased protection against virus variants compared to comparable concentrations of  
377 antibodies stimulated by vaccination.

378  
379 As additional variants of SARS-CoV-2 appear over time, individuals will acquire distinct  
380 immunological histories depending on which vaccines they received and which viral variants  
381 infected them. The idea that “imprinting” by a prior antigen exposure can shape, either positively  
382 or negatively, the response to a subsequent variant is well established in studies of influenza  
383 viruses, and has been implicated in birth-year differences in susceptibility to particular avian  
384 influenza viruses (Gostic et al., 2016). We find that prior vaccination with Wuhan-Hu-1-like  
385 antigens followed by infection with Alpha or Delta variants gives rise to plasma antibody  
386 responses with apparent Wuhan-Hu-1-specific imprinting manifesting as relatively decreased  
387 responses to the variant virus epitopes, compared to unvaccinated patients infected with those  
388 variant viruses. While current booster vaccinations are still based on the Wuhan-Hu-1-like  
389 antigens, vaccine manufacturers are in the process of evaluating updated vaccines encoding  
390 sequences from one or more circulating variants. Initial results from 3<sup>rd</sup> dose boosting with Beta  
391 spike-encoding mRNA vaccines after prior 2-dose mRNA-1273 vaccination are consistent with  
392 our findings of significant imprinting of serological responses by the first antigen encountered  
393 (Choi et al., 2021; Chu et al., 2021), indicating that vaccine-derived imprinting affects subsequent  
394 antibody responses stimulated by vaccination as well as infection. The extent to which vaccine  
395 boosting or infection with different variants will effectively elicit antibody responses to new  
396 epitopes, or rather increase responses to the epitopes of antigens encountered previously, as in the  
397 “original antigenic sin” phenomenon described for influenza virus infection and vaccination  
398 (Arevalo et al., 2020; Zhang et al., 2019), will be an important topic of ongoing study. The degree  
399 of imprinting may depend on the particular variants and the order in which they are introduced to  
400 the individual’s immune system, and the number of exposures, such as the number of vaccine

401 doses received. Additional data for evaluating the magnitude of these effects and their  
402 consequences for protection from infection are likely to become available in coming months, as  
403 individuals with different histories of SARS-CoV-2 vaccination or viral variant infection become  
404 infected with the more highly mutated Omicron variant ([https://covdb.stanford.edu/page/mutation-  
405 viewer/#omicron](https://covdb.stanford.edu/page/mutation-viewer/#omicron)). As a practical consideration, the very high spike-specific IgG concentrations  
406 generated by mRNA vaccination and periodic additional booster doses may be able to compensate  
407 for relatively decreased binding to new viral variant antigens, potentially decreasing the public  
408 health impact of antibody response imprinting if vaccine boosting is widely adopted.

409  
410 We hypothesized that differences in the serological responses observed in SARS-CoV-2 infection  
411 compared to vaccination, particularly those related to variant antigen binding breadth, could be  
412 related to the anatomical sites where the viral antigens are encountered, the quantity of viral  
413 antigens in those anatomical sites, differences in the cell populations stimulated in secondary  
414 lymphoid tissues, and potential damage to immunological tissues during infection. With CODEX  
415 multiplexed immunofluorescence microscopy and immunohistochemical microscopy, we  
416 identified follicular hyperplasia with robust axillary LN GCs after mRNA (BNT162b2 or mRNA-  
417 1273) vaccination, containing CD21<sup>+</sup> follicular dendritic cell networks, BCL6<sup>+</sup> B cells and PD-1<sup>+</sup>  
418 cells at significantly higher frequencies compared to those in peribronchial LNs of deceased  
419 COVID-19 patients. These findings demonstrate greater stimulation of GC B cells and Tfh cells  
420 in vaccination, and normal functional organization of GC follicular dendritic cells. Loss or  
421 impairment of GCs in patients with severe COVID-19 suggests that SARS-CoV-2 viral infection  
422 subverts the humoral immune response, by directly damaging immune cells or as a secondary  
423 effect of inflammatory responses to infection (Feng et al., 2020; Kaneko et al., 2020). The observed

424 extended presence of vaccine mRNA and spike protein in vaccinee LN GCs for up to 2 months  
425 after vaccination was in contrast to rare foci of viral spike protein in COVID-19 patient LNs. We  
426 hypothesize that the abundant spike antigen in the GCs of mRNA vaccine recipient LNs may  
427 contribute to the increased breadth of viral variant RBD binding by IgG seen after vaccination,  
428 potentially due to high antigen concentrations stimulating B cells with lower affinity for Wuhan-  
429 Hu-1 spike epitopes and better binding to variant epitopes. Persistent vaccine RNA and spike  
430 antigen at elevated concentrations in vaccinee LNs could result in less strict selection for higher-  
431 affinity B cells in the immune response compared to situations where antigen is more limiting  
432 (Cirelli et al., 2019). However, our observation that all vaccine modalities (mRNA, adenoviral and  
433 inactivated virus) stimulated greater viral variant breadth of IgG binding than infection could  
434 indicate that some other aspect of SARS-CoV-2 infection underlies these differences, such as  
435 alteration of GC function.

436  
437 Pre-pandemic analysis of a model RNA vaccine for yellow fever virus in a rhesus macaque at 16  
438 hours post-vaccination showed that vaccine RNA in LN cell suspensions was detected  
439 predominantly in professional antigen-presenting cells including monocytes, classical dendritic  
440 cells and B cells at this early time point (Lindsay et al., 2019). Data from follicular dendritic cells  
441 were not reported. Our histological data from SARS-CoV-2 mRNA-vaccinated humans at  
442 considerably later time points (7 to 60 days post-2<sup>nd</sup> dose) show vaccine RNA almost entirely in  
443 GCs, distributed primarily between the nuclei of GC cells, similar to the pattern seen by  
444 immunostaining for follicular dendritic cell processes or B cell cytoplasm. Additional co-  
445 localization studies with higher resolution may be required to determine more exactly which  
446 specific cell types harbor mRNA vaccine and spike antigen in humans following COVID-19

447 mRNA vaccination and infection, and may provide further mechanistic insights into the basis for  
448 the differences in serological responses after vaccination compared to infection.

449  
450 At least some portion of spike antigen generated after administration of BNT162b2 becomes  
451 distributed into the blood. We detected spike antigen in 96% of vaccinees in plasma collected one  
452 to two days after the prime injection, with antigen levels reaching as high as 174 pg/mL. The range  
453 of spike antigen concentrations in the blood of vaccinees at this early time point largely overlaps  
454 with the range of spike antigen concentrations reported in plasma in a study of acute infection  
455 (Ogata et al., 2020), although a small number of infected individuals had higher concentrations in  
456 the ng/mL range. At later time points after vaccination, the concentrations of spike antigen in blood  
457 quickly decrease, although spike is still detectable in plasma in 63% of vaccinees one week after  
458 the first dose. A practical finding in our study is that the detection of spike antigen in plasma  
459 samples is impeded after 2<sup>nd</sup> dose BNT162b2 vaccination, likely due to the formation of circulating  
460 immune complexes of anti-spike antibodies and spike protein, masking the antigen epitopes of the  
461 capture and detection antibodies that form the basis of antigen detection assays, similar to assay  
462 interference that has been reported for other diseases (Bollinger et al., 1992; Lima et al., 2014;  
463 Miles et al., 1993).

464

#### 465 *Limitations of the study*

466 Data from SARS-CoV-2 infected clinical cohorts and vaccinated individuals in this study are  
467 observational. Longitudinal data for COVID-19 vaccine responses are derived predominantly from  
468 BNT162b2 mRNA vaccine recipients at Stanford, with data for the other four COVID-19 vaccines  
469 at a single post-vaccination time point per individual. To make precise, internally controlled

470 comparisons of polyclonal antibody responses to different viral variant antigens, we used  
471 multiplexed ECL assays of antibody binding to RBD, rather than virus neutralization assays,  
472 therefore our data do not reflect potentially functional antibodies binding to the spike N-terminal  
473 domain, or antibodies that may have other activities *in vivo*. In the analysis of imprinting of  
474 serological responses, plasma specimens were not available from the period after vaccination but  
475 before variant virus infection, precluding direct comparison of antibody specificities pre- and post-  
476 infection. Additional epidemiological studies will be needed to evaluate the clinical impact of  
477 antibody response imprinting on susceptibility to infection by new viral variants, and the severity  
478 of disease in infected patients. LN histological comparisons between COVID-19 patients and  
479 vaccinees have the limitations that the infected patient specimens were limited to those with severe  
480 disease; the number of individuals analyzed was relatively low (six COVID-19 patients and seven  
481 vaccinees); and the LN sampling was not done prospectively at pre-determined time points after  
482 vaccination or infection. The serological analysis in this study is of polyclonal antibody responses;  
483 evaluation of the clonal B cell and plasma cell populations producing these antibody mixtures in  
484 comparable numbers of subjects in infection and vaccination will likely be required for further  
485 mechanistic understanding.

486

487 Taken together, these results underscore important differences between SARS-CoV-2 antibody  
488 responses produced by vaccination versus infection. Key questions for the months and years ahead  
489 include the duration of effective vaccine-stimulated serological responses after 3<sup>rd</sup> dose boosting  
490 or other repeated exposures, particularly for the recent Omicron variant and other variants that will  
491 emerge in future, and the safety and efficacy of variant-targeting vaccine boosters in previously  
492 vaccinated or infected individuals. Further mechanistic investigations into the differences in

493 antibody breadth elicited by vaccination and infection are needed to define the roles of T cell help,  
494 antibody affinity maturation, GC function, and innate immune responses to vaccine components,  
495 as well as the cellular and subcellular distribution of vaccine RNA and expressed antigen in  
496 lymphoid tissues. Lessons from the antibody responses to the initial SARS-CoV-2 variants are  
497 likely to be important both for preparing for future additional variants of this virus, as well as  
498 improving vaccination strategies for other pathogens such as influenza virus.

499

## 500 **Acknowledgments**

501 We acknowledge Lilit Grigoryan, Yupeng Feng, Meera Trisal, Florian Wimmers, and the Stanford  
502 Clinical and Translational Research Unit (CTRU) for their help in sample processing. We thank  
503 the research participants as well as the clinical staff who contributed to these studies. We thank  
504 ATUM (<https://www.atum.bio/>) for providing recombinant SARS-CoV-2 spike protein. The  
505 graphical abstract was created with BioRender.com.

506 Funding: This work was supported by NIH/NIAID R01AI127877, R01AI130398 and  
507 U19AI057229 (S.D.B.), a pilot project award from the Bill & Melinda Gates foundation (S.D.B.  
508 and S.C.A.N.), NIH/NCI 1U54CA260517 (S.D.B.), NIH/NIAID HHSN272201700013C (G.B.S.),  
509 NIH/NIA P30AG019610-20S1 (T.G.B.), an endowment to S.D.B. from the Crown Family  
510 Foundation, an anonymous philanthropic donation to the Boyd lab, an American Heart Association  
511 Postdoctoral Fellowship and Arnold O. Beckman Independence Award to M.J.S., an Early Postdoc  
512 Mobility Fellowship Stipend to O.F.W. from the Swiss National Science Foundation (SNSF), and  
513 an NSF Graduate Research Fellowship to M.Z.

514

## 515 **Author Contributions**

516 S.D.B., K.C.N., B.P., and M.M.D. conceptualized and designed the trial; K.R., S.C.A.N., O.S.,  
517 M.L.T., Y.N., and S.D.B. conceptualized and designed the study; A.S.L., M.M.S., J.L., and S.B.S.  
518 coordinated and performed blood collections under the supervision of K.C.N. and R.S.C.; C.C.,  
519 F.Y., O.F.W., R.A.H., P.S.A., E.H., A.S.L., M.M., I.C., F.G., V.M., C.L., and M.J.S. collected and  
520 processed samples; K.R., S.C.A.N., O.S., S.F.Y., O.F.W., D.S., A.W., D.C., and S.Z. performed  
521 the experiments; E.P., N.J.D., N.D.D., R.M., G.E.S., T.G.B., G.W.C., J.L.W., J.N.W., Y.N.,  
522 M.L.T., G.B.S., and B.A.P. provided reagents, and/or samples, and/or protocols; K.R., S.C.A.N.,  
523 O.S., S.F.Y., F.Y., M.Z., G.B.S., and S.D.B. analyzed the data and/or performed statistical  
524 analyses; K.R., S.C.A.N., O.S., and S.D.B. wrote the manuscript; all authors provided intellectual  
525 contributions, edited, and approved the manuscript.

526

#### 527 **Declaration of Interests**

528 S.D.B. has consulted for Regeneron, Sanofi, Novartis and Janssen on topics unrelated to this study,  
529 and owns stock in AbCellera Biologics. K.C.N. reports grants from National Institute of Allergy  
530 and Infectious Diseases (NIAID), Food Allergy Research & Education (FARE), End Allergies  
531 Together (EAT), National Heart, Lung, and Blood Institute (NHLBI), and National Institute of  
532 Environmental Health Sciences (NIEHS). K.C.N. is Director of FARE and World Allergy  
533 Organization (WAO) Center of Excellence at Stanford; Advisor at Cour Pharmaceuticals;  
534 Cofounder of Before Brands, Alladapt, Latitude, and IgGenix; National Scientific Committee  
535 member for the Immune Tolerance Network (ITN) of NIAID; recipient of a Research Sponsorship  
536 from Nestle; Consultant and Advisory Board Member at Before Brands, Alladapt, IgGenix,  
537 NHLBI, and ProBio; and Data and Safety Monitoring Board member at NHLBI. J.L.W., J.N.W.,  
538 and G.B.S. are employees of Meso Scale Diagnostics (MSD).

539 **Figure titles and legends**540 **Figure 1. Magnitude and duration of anti-SARS-CoV-2 IgG following BNT162b2**  
541 **vaccination and 3<sup>rd</sup> dose boost.**

542 (A) Anti-SARS-CoV-2 N, RBD, and spike (S) antibody responses are shown for plasma samples  
543 from individuals who received BNT162b2 prime (D0, n = 59 individuals), second dose (D21, n =  
544 58 individuals), and third dose (around month 9, n = 36 individuals) vaccination. Box-whisker  
545 plots of the anti-SARS-CoV-2 IgG concentrations in WHO BAU/mL show the interquartile range  
546 as the box and the whisker ends as the most extreme values within 1.5 times the interquartile range  
547 below the 25% quantile and above the 75% quantile. Red dashed lines indicate the cutoff values  
548 for positivity of each assay (MSD, package insert).

549 (B) Heatmap showing the development of antibody responses in longitudinal samples collected at  
550 D0, D7, D21, D28, D42, and D90/120 time points post-prime vaccination (x-axis). WHO BAU/mL  
551 Ig concentrations are displayed for study participants sorted by age (y-axis, color-coded). Rows  
552 are labeled on the right with “CoV-2+” for participants with a previous SARS-CoV-2 RT-qPCR  
553 positive test result.

554 (C) Correlations between anti-RBD and anti-spike IgG binding antibody concentrations in WHO  
555 BAU/mL and SARS-CoV-2 virus neutralization assays. Spearman rank correlation (coefficient =  
556 Rho, displayed in the plot for each assay comparison) was used to assess the strength of correlation  
557 between binding antibody concentrations and virus neutralization results. Red dashed lines  
558 indicate the cutoff values for positivity of each assay (MSD, package insert).

559

560 **Figure 2. BNT162b2 vaccination and SARS-CoV-2 infection elicit distinct Ig isotype profiles.**

561 (A, B) Anti-SARS-CoV-2 N, RBD, and spike (S) IgM, IgG, and IgA antibody responses are shown

562 for individuals who received BNT162b2 prime (D0) and 2<sup>nd</sup> (D21) vaccination doses and for  
563 COVID-19 patients.

564 (A) The heatmap shows the development of antibody responses in longitudinal samples from  
565 vaccinees/patients collected at D0, D7 / week 1, D21 / weeks 2&3, D28 / week 4, D42 / weeks  
566 5&6, and D90/120 /  $\geq$ week 7 after vaccination / COVID-19 symptom onset (x-axis). The color  
567 scale encodes the median values of log<sub>10</sub> WHO BAU/mL Ig concentrations.

568 (B) Box-whisker plots show the development of antibody responses in longitudinal samples from  
569 vaccinees / patients collected at D0, D7 / week 1, D21 / weeks 2&3, D28 / week 4, D42 / weeks  
570 5&6, and D90/120 /  $\geq$ week 7 after vaccination / COVID-19 symptom onset (x-axis). Box-whisker  
571 plots show the interquartile range as the box and the whisker ends as the most extreme values  
572 within 1.5 times the interquartile range below the 25% quantile and above the 75% quantile.  
573 Statistical test: pairwise Wilcoxon rank sum test with Bonferroni correction. \* $p < 0.05$ , \*\* $p < 0.01$ ,  
574 \*\*\* $p < 0.001$ .

575 Individuals were classified as outpatients (Outpt) and hospital admitted patients (Admit); intensive  
576 care unit (ICU) patients and those who died from their illness (Death); and vaccinees who had  
577 (CoV-2+) or had not had a positive SARS-CoV-2 test in the past.

578 (C) PCA of anti-SARS-CoV-2 RBD, N-terminal domain, and S (but not N) IgM, IgG, and IgA  
579 concentrations across BNT162b2 vaccinees and Wuhan-Hu-1-infected Stanford COVID-19  
580 patient cohort 1 at different time points after vaccination / COVID-19 symptom onset visualized  
581 on a consistent PCA reference created using D21 / weeks 2&3 as a reference time point.

582 (D) Distribution of Euclidean distances between BNT162b2 vaccinee samples and their centroid,  
583 compared to Wuhan-Hu-1-infected Stanford COVID-19 patient cohort 1 samples and their  
584 centroid, at different time points after vaccination / COVID-19 symptom onset.

585 **Figure 3. Greater breadth of IgG binding to SARS-CoV-2 RBD variants following**  
586 **BNT162b2 vaccination compared to infection with Wuhan-Hu-1 SARS-CoV-2.** Anti-SARS-  
587 CoV-2 Wuhan-Hu-1 and viral variant RBD IgG responses are shown for Stanford individuals who  
588 received BNT162b2 vaccination and for Wuhan-Hu-1-infected COVID-19 Stanford patient cohort  
589 1 at different time points after vaccination / COVID-19 symptom onset. Box-whisker plots show  
590 the interquartile range as the box and the whisker ends as the most extreme values within 1.5 times  
591 the interquartile range below the 25% quantile and above the 75% quantile. Significance between  
592 patient and vaccinee groups were tested with two-sided Wilcoxon rank sum test. \* $p < 0.05$ , \*\* $p <$   
593  $0.01$ , \*\*\* $p < 0.001$ .

594 (A) Anti-RBD IgG concentrations.

595 (B) Ratios of anti-Wuhan-Hu-1 to variant RBD IgG concentration.

596

597 **Figure 4. Greater breadth of IgG binding to SARS-CoV-2 variant RBDs following**  
598 **vaccination with four different vaccines compared to infection with Wuhan-Hu-1 SARS-**  
599 **CoV-2.** Anti-SARS-CoV-2 Wuhan-Hu-1 and viral variant RBD IgG responses are shown for  
600 individuals who received BNT162b2 (BioNTech-Pfizer), ChAdOx1-S (AstraZeneca), Gam-  
601 COVID-Vac (Sputnik V), and BBIBP-CorV (Sinopharm) vaccination and for Wuhan-Hu-1-  
602 infected COVID-19 Stanford patient cohort 2 within one month and around three months after  
603 vaccination / COVID-19 symptom onset. Box-whisker plots show the interquartile range as the  
604 box and the whisker ends as the most extreme values within 1.5 times the interquartile range below  
605 the 25% quantile and above the 75% quantile. Significance between groups were tested with  
606 pairwise Wilcoxon rank sum test with Bonferroni correction. \* $p < 0.05$ , \*\* $p < 0.01$ , \*\*\* $p < 0.001$ .

607 (A) Anti-RBD IgG concentrations.

608 (B) Ratios of anti-Wuhan-Hu-1 to variant RBD IgG concentration.

609

610 **Figure 5. Variant-specific serological signature following Alpha and Delta SARS-CoV-2**  
611 **infection.**

612 (A) Anti-Wuhan-Hu-1 to variant RBD IgG concentration ratios are shown for individuals with  
613 primary SARS-CoV-2 Alpha or Delta variant infection (upper panels) or secondary variant  
614 infection after vaccination (lower panels). Box-whisker plots show the interquartile range as the  
615 box and the whisker ends as the most extreme values within 1.5 times the interquartile range below  
616 the 25% quantile and above the 75% quantile.

617 (B) Anti-SARS-CoV-2 variant IgG binding preference levels of BNT162b2 vaccinees on day 28  
618 post vaccination and of previously vaccinated or nonvaccinated individuals infected with the  
619 SARS-CoV-2 Delta variant.

620

621 **Figure 6. Disrupted LN GCs in COVID-19 patients versus mRNA vaccinees.**

622 (A) Representative LN GC histology of COVID-19 patients and vaccinees evaluated with 4-color  
623 CODEX immunofluorescence analysis for CD20 (B cells), CD3 (T cells), BCL6 (GC B cells  
624 (major subset) and follicular helper T cells (minor subset)), and CD21 (follicular dendritic cells).

625 (B) Representative immunohistochemistry of GCs with CD21 (left), BCL6 (middle) and PD-1  
626 (right) in peribronchial LNs of an autopsy patient who died of COVID-19, a control autopsy patient  
627 who died from a non-COVID-19 pneumonia (pre-pandemic), and in an axillary LN of a patient  
628 vaccinated with a SARS-CoV-2 mRNA vaccine.

629 (C-E) Relative proportion (upper) and absolute number (lower) of GCs in LNs (C), of BCL6+ cells  
630 within GCs (D), and of PD-1+ cells within GCs (E) from COVID-19 autopsy patients (n = 6),

631 control autopsy patients (n = 3), and mRNA vaccinated patients (n = 7). Quantification performed  
632 in QuPath digital pathology analysis software. Wilcoxon rank sum test was used to calculate p  
633 values. Error bars represent mean  $\pm$  SEM. \*p < 0.03; \*\*p < 0.003.

634

635 **Figure 7. Localization of SARS-CoV-2 proteins and vaccine mRNA in LNs.**

636 (A) Representative LN GC after mRNA vaccination showing Hematoxylin & Eosin staining  
637 (upper left), 4-color CODEX staining (lower left), *in situ* hybridization of a SARS-CoV-2 mRNA  
638 vaccine-specific probe (upper right (lower magnification) and middle right (greater  
639 magnification)), and immunohistochemical (IHC) staining for spike antigen (lower right). Vaccine  
640 mRNA probe hybridization was visualized by colorimetric development with Fast Red  
641 chromogen, and positive IHC staining for spike antigen was visualized as granular brown color  
642 from 3,3'-Diaminobenzidine (DAB) reagent.

643 (B) Representative *in situ* hybridization of an RNAScope control probe (left panels) and SARS-  
644 CoV-2 mRNA vaccine-specific probe (middle panels) within ipsilateral axillary core needle LN  
645 biopsies of female patients 7 to 60 days after second mRNA-1273 or BNT162b2 dose. Probe  
646 hybridization is indicated by red chromogen spots. IHC signal for spike antigen (right panels), is  
647 detected as granular brown staining.

648 (C) Quantification of SARS-CoV-2 mRNA vaccine-specific probe-staining GCs in vaccinated LN  
649 biopsies.

650 (D) Quantification of positive SARS-CoV-2 mRNA vaccine-specific probe spots per GC in  
651 vaccinee LNs. Error bars represent mean  $\pm$  SEM.

652 (E) Spike protein-positive GC quantification from IHC staining of vaccinee LNs.

653 (F) IHC staining for spike (lower right panel) and nucleocapsid (upper panels and lower left panel)  
654 antigens in representative sections of COVID-19 patient peribronchial LNs. Nucleocapsid  
655 detection in primary (upper right panel) and secondary (upper left panel) LN follicles.

656 (G) Due to the low frequency of detection of spike antigen in COVID-19 patient LNs,  
657 quantification is presented as the number of patients with positive staining in their LN specimens.

658 (H) Quantification of the number of COVID-19 patients with LN follicles positive for  
659 nucleocapsid IHC staining.

660 (I) Number and percentage of nucleocapsid-positive follicles by IHC in COVID-19 patient LNs.  
661 Error bars represent mean  $\pm$  SEM.

662 (J) Spike concentration measured in plasma samples collected before and at several time points  
663 after BNT162b2 vaccination, with the red dotted line indicating the cutoff for positive.

664 (K) Spike concentrations were measured in plasma samples collected from BNT162b2 vaccinees  
665 on D0 (spike negative) or D28 (spike positive) spiked with different concentrations of recombinant  
666 spike protein. Black dotted line = cutoff for positive.

667 (L) Spike concentration measured in plasma samples collected from BNT162b2 vaccinees on D0,  
668 D21, D22/23, and D28 mixed with the same plasma sample collected from one BNT162b2  
669 vaccinee on D1 (spike positive). Black dotted line = cutoff for positive.

670

671 **STAR Methods**672 **RESOURCE AVAILABILITY**673 *Lead Contact*

674 Further information and requests for resources and reagents should be directed to the Lead Contact,  
675 Dr. Scott D. Boyd ([publications\\_scott\\_boyd@stanford.edu](mailto:publications_scott_boyd@stanford.edu)).

676

677 *Materials Availability*

678 This study did not generate new unique reagents.

679

680 *Data and Code Availability*

681 Raw data from all serology Figures have been deposited on Mendeley at  
682 <http://dx.doi.org/10.17632/j8r94pfrj6.1> and are publicly available as of the date of publication. All  
683 original code has been deposited on the Zenodo platform at  
684 <https://doi.org/10.5281/zenodo.5854880> and is publicly available at the Github repository  
685 <https://github.com/boyd-lab/covid-infection-vs-vaccination> as of the date of publication. Any  
686 additional information required to reanalyze the data reported in this paper is available from the  
687 lead contact upon request.

688

689 **EXPERIMENTAL MODELS AND SUBJECT DETAILS**690 *Plasma and saliva samples from Stanford BNT162b2 vaccinees*

691 To study antibody responses after first, second, and third dose vaccination with BNT162b2, we  
692 collected longitudinal blood and saliva samples from 59 vaccinees (29 were women, 27 were men,  
693 3 were unknown, and all donors were adults between the ages of 19 to 79 years). Baseline blood

694 samples were collected on day 0 before or immediately after the first vaccine dose. Individuals  
695 received their second dose on day 21 and a third dose about 9 months after the prime. Blood sample  
696 collection after prime vaccination was scheduled for days 1, 7, 21, 22, 28, and 42 with blood draws  
697  $\pm$  one day from the assigned time point, or days 90, 120, or 210  $\pm$  1 week from the assigned time  
698 point. In addition, blood samples were collected on days 0 to 3, 7 to 10, 21, and 28 after the third  
699 vaccine dose. Saliva samples were collected on day 42 after the first dose, as well as before, and 1  
700 or 2, 3 or 4, 7, and 21 days after the third vaccine dose. Peripheral blood was collected in vacutainer  
701 cell preparation tubes (CPTs) containing sodium citrate. Plasma was isolated and stored at  $-80^{\circ}\text{C}$ .  
702 Saliva was collected from study participants, centrifuged, and supernatants were stored at  $-80^{\circ}\text{C}$ .  
703 All BNT162b2 vaccine study participants provided informed consent under Stanford University  
704 Institutional Review Board approved protocol IRB-55689.

705

#### 706 *Plasma and saliva samples from Stanford COVID-19 patients*

707 Blood and saliva samples were collected between March and December 2020 from COVID-19  
708 patients who reported to Stanford Healthcare-associated clinical sites. SARS-CoV-2 infection was  
709 confirmed for all patients by RT-qPCR of nasopharyngeal swabs as described (Corman et al.,  
710 2020; Hogan et al., 2020). Blood samples were collected in heparin- or EDTA-coated vacutainers.  
711 After centrifugation for collection of plasma or saliva, samples were stored at  $-80^{\circ}\text{C}$ . The use of  
712 these samples for antibody testing was approved by the Stanford University Institutional Review  
713 Board (Protocols IRB-48973 and IRB-55689).

714 **Stanford COVID-19 patient cohort 1** included 530 plasma samples collected from 100  
715 moderately to severely ill COVID-19 patients (52 were women and 48 were men; ages ranged  
716 from 1 to 95 years; 23 were outpatients, 33 were admitted to hospital without needing ICU care,

717 20 were treated in the ICU and 24 died of COVID-19) between March 2020 and August 2020.  
718 ELISA serology data for Wuhan-Hu-1 SARS-CoV-2-specific antibodies in these specimens have  
719 been reported previously (Röltgen et al., 2020).

720 **Stanford COVID-19 patient cohort 2** was included as a validation cohort of 87 samples from 74  
721 mostly mildly ill patients who had blood sample draws between March and December 2020, at  
722 approximately 21 days (n = 15 samples), 1 month (n = 23 samples), 3 months (n = 27 samples)  
723 and 7 months (n = 22 samples) after positive RT-qPCR testing for SARS-CoV-2 infection. Of  
724 those patients, 37 were women, 34 were men and 3 were unknown. Donors were 19 to 72 years of  
725 age and in terms of disease severity, 59 were mildly ill, 6 were moderate ill and 9 had a  
726 severe/critical disease course. Specimen time points were selected to match those of Stanford  
727 BNT162b2 vaccinee sample collections. Saliva samples were collected from five COVID-19  
728 patients.

729 **Stanford SARS-CoV-2 variant infection cohort** blood samples were collected from COVID-19  
730 patients during acute infection with SARS-CoV-2 Alpha (n = 7) or Delta (n = 34) variants. Samples  
731 were from 20 women and 21 men, all between 2 and 92 years of age. SARS-CoV-2 genotyping  
732 data were obtained using a multiplex, mutation-specific RT-qPCR targeting N501Y, E484K, and  
733 L452R, as previously described (Wang et al., 2021). Samples from the first multiplexed reaction  
734 suspected to contain the Alpha variant were analyzed with a second confirmatory genotyping RT-  
735 qPCR assay to detect mutations encoding the N501Y amino acid change, as described (Dashdorj  
736 et al., 2021a).

737

738 ***Plasma samples from Mongolian vaccinees***

739 To study SARS-CoV-2 variant-specific IgG responses elicited by different COVID-19 vaccines,  
740 we tested plasma samples collected in July 2021 from 196 Mongolian vaccine study participants  
741 (109 were women, 87 were men, all were adults between 20 and 85 years of age) who had been  
742 fully vaccinated with one of four COVID-19 vaccines: BioNTech-Pfizer BNT162b2 (n = 47),  
743 AstraZeneca ChAdOx1-S (n = 50), Sputnik V Gam-COVID-Vac (n = 45) and Sinopharm BBIBP-  
744 CorV (n = 54). Participants were recruited by public announcement and volunteers were enrolled  
745 after signing the consent form approved by the Ethics Review Board at the Ministry of Health of  
746 Mongolia. SARS-CoV-2 pseudotyped virus neutralization and RBD-ACE2 blocking data on the  
747 same samples have been reported previously (Dashdorj et al., 2021a). Peripheral blood was  
748 collected in CPT, centrifuged for collection of plasma, and stored at -80°C.

749

750 ***Healthy human control (HHC) plasma and saliva***

751 37 plasma and 20 saliva samples from HHCs collected before the onset of the COVID-19  
752 pandemic for studies at the Sean N. Parker Center for Allergy & Asthma Research were used to  
753 verify pre-pandemic antibody binding concentrations to the different coronavirus antigens, and  
754 manufacturer-provided cutoffs for positive serology assay results. Use of these samples was  
755 approved by the Stanford University Institutional Review Board (Protocols IRB-8629 and IRB-  
756 60171). No demographic information was available for these samples.

757

758 ***Axillary LN core biopsies and post-mortem peribronchial LN tissues***

759 To analyze and compare GC architecture in response to COVID-19 vaccination and SARS-CoV-  
760 2 infection, we collected axillary LN core needle biopsies from BNT162b2 or mRNA-1273

761 vaccinees, and excised post-mortem peribronchial LNs from patients who died of COVID-19. For  
762 the selection of vaccinee tissues, we performed a retrospective search of our pathology archives  
763 and medical records between January 2021 and June 2021 for female patients who received either  
764 mRNA-1273 or BNT162b2 vaccination and subsequently underwent an ipsilateral axillary LN  
765 core needle biopsy due to mammographic findings and routine clinical care. Seven patients  
766 underwent biopsy one to eight weeks after vaccination with their second dose of mRNA vaccine.  
767 Three unvaccinated females undergoing axillary LN core biopsy for routine clinical care and  
768 mammographic findings served as controls. We included six peribronchial LNs from two female  
769 and four male patients who died of COVID-19 before August 2020, one to three weeks after  
770 symptom onset. Control post-mortem peribronchial LN biopsies were from pre-pandemic patients  
771 who died of non-COVID-19 causes. Autopsies were done by the Arizona Study of Aging and  
772 Neurodegenerative Disorders Brain and Body Donation Program (Beach et al., 2015). Analysis of  
773 these tissues was approved by Stanford University Institutional Review Board Protocol IRB-  
774 48973.

775

## 776 **METHOD DETAILS**

### 777 *MSD ECL binding assays*

778 Plasma samples from vaccinees and COVID-19 patients were heat-inactivated at 56°C for 30  
779 minutes and tested using multiplexed ECL detection in a 96-well plate format with MSD® V-  
780 PLEX® serology panels and instrumentation according to the manufacturer's instructions. V-  
781 PLEX COVID-19 Coronavirus Panel 2 kits were used to detect IgM, IgG, and IgA antibodies to  
782 SARS-CoV-2 N, S1 NTD, RBD, and spike antigens and to spike proteins of SARS-CoV and other  
783 HCoVs including HCoV-OC43, HCoV-HKU1, HCoV-NL63, and HCoV-229E. V-PLEX SARS-

784 CoV-2 Panel 9 and 11 kits were used to determine IgG antibody concentrations and RBD-ACE2  
785 blocking antibody percentages to different SARS-CoV-2 variant RBDs, with Alpha, Beta, Gamma,  
786 Epsilon, Kappa, Eta/Iota, B.1.526.2, P.3 and Wuhan-Hu-1 present in both panel 9 and 11, and with  
787 B.1.214.2 in panel 9 and Delta in panel 11. V-PLEX SARS-CoV-2 Panel 20 kits were used to  
788 determine IgG antibody concentrations to Alpha, Beta, Gamma, Delta, and Wuhan-Hu-1 SARS-  
789 CoV-2 variant spike proteins. Plasma samples were analyzed in duplicate at a 1:5,000 (for IgG  
790 binding assays) or a 1:10 (for RBD-ACE2 blocking assays) dilution in MSD diluent. Coronavirus-  
791 specific antibodies were detected with anti-human IgM, IgG, or IgA antibodies, or indirectly with  
792 human ACE2 protein (for RBD-ACE2 blocking assays) conjugated to SULFO-TAG™ ECL labels  
793 and read with a MESO® QuickPlex® SQ 120 instrument. Cutoff values for positive antibody test  
794 results for Wuhan-Hu-1 antigens were determined by the manufacturer based on sera from 200  
795 pre-pandemic healthy adults and 214 PCR-confirmed COVID-19 patients. We tested an additional  
796 37 healthy adult pre-pandemic plasma specimens to evaluate the manufacturer's cutoff values, and  
797 to determine cutoffs for positive binding to variant virus antigens, defined as the mean plus three  
798 standard deviations of the results from the pre-pandemic specimens. Antibody binding ratios for  
799 Wuhan-Hu-1 and viral variant antigens were only calculated for specimens that were above the  
800 cutoff values for positive results. Saliva samples were analyzed in duplicate at a 1:5 dilution in  
801 MSD diluent 2. Each plate contained duplicates of a 7-point calibration curve with serial dilution  
802 of a reference standard, a blank well and three positive control samples. Calibration curves were  
803 used to calculate antibody unit concentrations by backfitting ECL signals measured for each  
804 sample to the curve.

805

806 ***MSD ECL spike antigen detection***

807 SARS-CoV-2 spike antigen was quantified in plasma samples using an antigen capture ECL  
808 immunoassay platform (Meso Scale Discovery). S-PLEX<sup>®</sup> SARS-CoV-2 spike Kit assays were  
809 performed according to manufacturer instructions. A 7-point calibration curve and negative control  
810 consisting of assay diluent were run in duplicate on each plate. Plates were read using a MESO  
811 QuickPlex SQ 120 instrument. Raw signals were converted to a concentration based on linear  
812 regression to the 7-point calibration curve. Recombinant SARS-CoV-2 spike protein used for  
813 plasma spiking experiments was made by ATUM (<https://www.atum.bio/>).

814

### 815 ***Histology, immunohistochemistry & in situ hybridization***

816 LN core needle and autopsy tissue samples were fixed in formalin and embedded in paraffin  
817 (FFPE), and sectioned. Once unstained slides were generated and initial Hematoxylin and Eosin  
818 (H&E) stained sections were analyzed, two distinct 0.6 mm areas from each LN sample were cored  
819 out of each tissue block and re-embedded to construct a tissue microarray (TMA).  
820 Immunohistochemistry was performed on four-micron sections using standard automated or  
821 manual methods including deparaffinization, peroxidase blocking, antigen retrieval, primary and  
822 secondary antibody incubation, detection with 3,3'-Diaminobenzidine (DAB) development, and  
823 counterstaining. Assays were performed on Roche Ventana (Tucson, AZ) Ultra instruments using  
824 Ventana Optiview detection, or Leica (Buffalo Grove, IL) Bond III instruments using Leica  
825 Polymer Refine detection or manually using Dako (Carpenteria, CA) Target Retrieval (TR) and  
826 Liquid DAB+ Substrate Chromogen System with ImmPress (Vector, Burlingame, CA) secondary  
827 antibodies.

828 For *in situ* hybridization, manual methods were used as previously described (Cloutier et al., 2021),  
829 using manufacturer-recommended protocols with the RNAScope 2.5 HD Assay-RED kit and

830 probes from Advanced Cell Diagnostics (Newark, CA). Two SARS-CoV-2 vaccine probes were  
831 developed to target bases 101-1143 of the spike encoding sequence of the BNT162b2 vaccine or  
832 bases 101-1488 of the spike encoding sequence of the mRNA-1273 vaccine. Both probes  
833 recognized SARS-CoV-2 mRNA vaccine, thus only the SARS-CoV-2 vaccine probe recognizing  
834 bases 101-1488 of mRNA-1273 vaccine are presented. To assess the specificity of SARS-CoV-2  
835 RNAScope vaccine probes, they were tested against SARS-CoV-2 infected placental tissue, in  
836 addition to staining for SARS-CoV-2 viral probe which targets bases 21631-23303 of the S-gene.  
837 SARS-CoV-2 RNAScope vaccine probes did not recognize SARS-CoV-2 virus. In addition, for  
838 each tissue tested there were internal negative control areas which did not react with SARS-CoV-  
839 2 vaccine probe.

840

#### 841 ***Whole Slide Imaging (WSI) and Quantitative Image Analysis***

842 Whole slide images of immunohistochemistry-stained slides for BCL6, PD-1 and CD21 were  
843 scanned at 40X magnification (0.25  $\mu\text{m}$  per pixel) on an Aperio AT2 scanner (Leica Biosystems,  
844 Nussloch, Germany) in ScanScope Virtual Slide (SVS) format. Total lymphoid tissue and  
845 individual GCs were annotated as regions of interests (ROIs) using the QuPath open-source WSI  
846 software (Bankhead et al., 2017). GCs were defined as B cell areas with CD21+ follicular dendritic  
847 cell networks and BCL6+ nuclei. Primary follicles were defined as B cell areas with CD21+  
848 follicular dendritic cell networks without BCL6+ nuclei. For each GC ROI, the standard positive  
849 cell detection function was used to identify positive and negative cells with a single threshold of  
850 0.2 when scoring the cell DAB OD mean. For autopsy BCL6 analysis (COVID-19 and control)  
851 the threshold was adjusted to 0.05 given the dim expression of BCL6. For each ROI, the area in  
852  $\text{mm}^2$ , number positive cells per  $\text{mm}^2$ , and percent positive cells were calculated by QuPath.

853 A TMA slide containing two distinct 0.6 mm cores of each of the mRNA vaccine (n = 7) and  
854 vaccine control (n = 3) biopsies hybridized with SARS-CoV-2 mRNA RNAScope vaccine probe  
855 was scanned at 40X magnification (0.25  $\mu\text{M}$  per pixel) on an Aperio AT2 scanner in SVS format.  
856 Total lymphoid tissue and individual GCs were annotated as ROIs using QuPath. For each GC  
857 ROI, the number of spots/clusters of RNAScope probe were detected using the QuPath subcellular  
858 detection option per manufacture instructions. Our detection parameters were as follows:  
859 Detection threshold = 0.6; split by intensity. Our split and cluster parameters were as follows:  
860 expected spot size = 2  $\mu\text{m}^2$ , min spot size = 2  $\mu\text{m}^2$ , max spot size = 3  $\mu\text{m}^2$ .

861

#### 862 *Co-detection by indexing (CODEX)*

863 All antibodies used for CODEX were first screened, titrated, and validated by individual staining  
864 on FFPE human tonsil tissue samples. Standard manual immunohistochemistry was used to cross-  
865 validate antibodies with the same, non-conjugated antibody clones listed in the key resource table.  
866 Tissue preparation for CODEX was undertaken by obtaining eight-micron thick sections from  
867 FFPE tissue blocks which were immobilized on charged square glass coverslips coated with  
868 polylysine (Electron Microscopy Sciences, Hatfield, PA) prepared according to the manufacturer's  
869 instructions. The coated glass coverslips were stained with a cocktail containing nucleotide-  
870 barcoded primary antibodies. The coverslips underwent nuclear staining (DAPI) and were loaded  
871 on the stage of an automated inverted fluorescence microscope connected to the robotic fluidic  
872 system known as CODEX (Akoya biosciences, Marlborough, MA). In addition to the nuclear stain,  
873 fluorophore-tagged complementary nucleotide sequences (reporters) were used to iteratively  
874 reveal three antibodies at a time per cycle. Two additional blank cycles at the beginning and at the  
875 end of the antibody reveal cycles were added for purposes of subtraction of auto-fluorescence

876 background. Automated image acquisition, processing, segmentation, and fluidics exchange were  
877 conducted using an Akoya CODEX instrument and CODEX driver software (Akoya biosciences)  
878 (Black et al., 2021; Goltsev et al., 2018; Schürch et al., 2020). Composite images providing  
879 multiplex fluorescent signals of stained cell types, cellular niches, and tissue architecture were  
880 captured using CODEX® MAV and FIJI software (Akoya biosciences).

881

## 882 **QUANTIFICATION AND STATISTICAL ANALYSIS**

883 Statistical tests were performed in R using base packages for statistical analysis and the ggplot2  
884 package for graphics. Box-whisker plots show median (horizontal line), interquartile range (box),  
885 and the end of the lower whisker representing the smallest observation greater than or equal to the  
886 25% quantile minus 1.5 times the interquartile range, and the end of the upper whisker representing  
887 the largest observation less than or equal to the 75% quantile plus 1.5 times the interquartile range.  
888 In serological analyses where statistical significance was tested, significance was defined as: \*\*\*p  
889 value < 0.001; \*\*p value < 0.01; \*p value ≤ 0.05.

890 For the principal component analysis (PCA) we log-transformed, calculated z-scores, and ran PCA  
891 on MSD antibody concentration measurements or Wuhan-Hu-1/variant RBD IgG concentration  
892 ratios from a reference time point after COVID-19 vaccination or SARS-CoV-2 infection using  
893 Python v3.7.10 and packages numpy v1.19.1, pandas v1.2.5, and scikit-learn v1.0. We then applied  
894 these transformations to matching data from all other time points, enabling us to visualize the  
895 change over time in these serology measurements on a consistent PCA reference. Plots were  
896 created with Python packages matplotlib version 3.3.2 and seaborn version 0.11.2.

897

898 For the analysis of the homogeneity or dispersion of serology measurements in groups differing  
899 by vaccination or infection status (Figures 2C and 2D) at a particular time point, we plotted each  
900 group's distribution of Euclidean distances to its centroid (calculated with Python package scipy  
901 version 1.6.2). These distance distributions were consistent when calculated in the raw  
902 measurement data space of arbitrary units (AU) for the MSD ECL assay or in the transformed PC1  
903 and PC2 space after embedding the raw measurements into the PCA space created from one  
904 reference time point.

905  
906 Ratios of concentrations of IgG binding to Wuhan-Hu-1 RBD compared to variant virus RBDs  
907 were plotted for specimens with IgG binding above the cutoff for positive binding to Wuhan-Hu-  
908 1 RBD (Figures 3, 4 and S4) to avoid distortion of ratios by samples without specific binding.  
909 Ratios of IgG binding to spike antigens were calculated in a similar manner (Figure S4C, lower  
910 panel). Corresponding IgG concentrations for samples used to calculate ratios were plotted for  
911 reference (Figures 3A, 4A, S4A and S4C upper panel). To quantify serological imprinting from  
912 prior Wuhan-Hu-1 antigen exposure from vaccination on subsequent responses to breakthrough  
913 infection with the Delta variant, we first computed the ratio of Wuhan-Hu-1 RBD binding level to  
914 Delta RBD binding level. Here, a ratio of one indicates even preference, while ratios greater than  
915 one indicate preferential binding of Wuhan-Hu-1 over Delta. Each ratio is symmetric with its  
916 inverse; for example, a Wuhan-Hu-1/Delta binding ratio of  $4/5$  indicates the same degree of  
917 preference for Delta binding as the ratio  $5/4$  indicates for Wuhan-Hu-1 binding preference. We  
918 then log-transformed the ratios, which sets the even preference level at zero, with positive values  
919 corresponding to Wuhan-Hu-1 preference, and makes these values symmetric around zero (e.g., a  
920 value of  $-0.2$  indicates the same level of preference for Delta as  $+0.2$  does for Wuhan-Hu-1

921 binding). Finally, we rescaled the negative and positive values separately to the ranges -100% to  
922 0 and 0 to +100%. The resulting magnitudes are binding preferences relative to the maximum  
923 binding preference observed for a particular variant, including data from individuals only exposed  
924 to Wuhan-Hu-1 or individual variants. In particular, -100% refers to the maximum observed  
925 binding preference towards Delta. We plotted the distributions of these binding preference levels  
926 for BNT162b2 vaccinees without known prior SARS-CoV-2 infection, for Delta infection cases  
927 with no recorded prior infection or vaccine exposure, and for Delta breakthrough infections  
928 following Wuhan-Hu-1 wild-type vaccination. An example binding preference level of +30% for  
929 a Delta breakthrough infection case suggests this individual is at 30% of the most imprinted state  
930 for Wuhan-Hu-1 preference. A binding preference of -20% would instead suggest that, following  
931 infection, this individual lost imprinting to Wuhan-Hu-1 and gained preference for binding the  
932 Delta variant.

933

#### 934 **Supplemental information titles and legends**

935 **Figure S1. Anti-SARS-CoV-2 Ig antibody responses in plasma and saliva following**  
936 **BNT162b2 vaccination, related to Figure 1.**

937 Anti-SARS-CoV-2 N, RBD, and spike (S) IgG (A), IgM (B), and IgA (C) responses are shown for  
938 plasma from individuals who received BNT162b2 prime (D0, n = 59) and second dose (D21, n =  
939 58) vaccination. Box-whisker plots of the WHO binding arbitrary unit (BAU/mL) anti-SARS-  
940 CoV-2 concentrations show the interquartile range as the box and the whisker ends as the most  
941 extreme values within 1.5 times the interquartile range below the 25% quantile and above the 75%  
942 quantile. Comparisons between groups of previously SARS-CoV-2-infected (CoV-2+) versus non-  
943 infected individuals and female versus male were by the two-sided Wilcoxon rank sum test;

944 comparison between age groups (< 40; 40 to 60; > 60 years) was done using pairwise Wilcoxon  
945 rank sum test with Bonferroni correction. \* $p < 0.05$ , \*\* $p < 0.01$ , \*\*\* $p < 0.001$ .  
946 (D) Anti-SARS-CoV-2 N, RBD, and S IgG concentrations in BAU/mL are shown for saliva from  
947 individuals who received BNT162b2 prime/boost and 3<sup>rd</sup> dose vaccination (upper left panel). Anti-  
948 SARS-CoV-2 N, RBD, and S (upper right panel) concentrations in BAU/mL, as well as anti-  
949 SARS-CoV-1 and anti-HCoV-OC43, -HKU1, -NL63, and -229E S IgG (lower panel)  
950 concentrations in MSD arbitrary units (AU/mL) are shown for saliva collected on D42 after  
951 BNT162b2 prime vaccination (vaccinee), around D42 post-symptom onset for COVID-19 patients  
952 (CoV-2+), and before the onset of the COVID-19 pandemic for pre-pandemic healthy human  
953 controls (Pre-pan). Box-whisker plots of anti-SARS-CoV-2 IgG concentrations show the  
954 interquartile range as the box and the whisker ends as the most extreme values within 1.5 times  
955 the interquartile range below the 25% quantile and above the 75% quantile. Statistical test for  
956 significance between groups (CoV-2+; Pre-pan, Vaccinee) was performed using pairwise  
957 Wilcoxon rank sum test with Bonferroni correction. \* $p < 0.05$ , \*\* $p < 0.01$ , \*\*\* $p < 0.001$ .

958

959 **Figure S2. The magnitude of antibody responses is not correlated with reported vaccine-**  
960 **associated side effects (SEs), related to Figure 1.**

961 (A) Frequency of site-specific and systemic vaccine-associated SEs after prime (light green) and  
962 second dose (dark green) BNT162b2 vaccination.

963 (B) Box-whisker plots of the MSD AU/mL anti-SARS-CoV-2 IgG concentrations in BNT162b2  
964 vaccinee plasma collected on D28 post-vaccination show the interquartile range as the box and the  
965 whisker ends as the most extreme values within 1.5 times the interquartile range below the 25%  
966 quantile and above the 75% quantile. For a given SE (rows), vaccinees were grouped according to

967 no SE reported (“No”, colored in blue) or SE reported (“Yes”, colored in orange). Vaccinees where  
968 SEs were unknown are shown as white boxplots.

969

970 **Figure S3: BNT162b2 vaccination produces less broad serological responses to endemic**  
971 **HCoVs compared to SARS-CoV-2 infection, related to Figure 2.**

972 (A, B) Anti-SARS-CoV-1 spike, and anti-HCoV-OC43, -HKU1, -NL63, and -229E spike IgM,  
973 IgG, and IgA antibody responses are shown for individuals who received BNT162b2 prime (D0)  
974 and boost (D21) vaccination doses and for COVID-19 patients.

975 (A) The heatmap shows the development of antibody responses in longitudinal samples from  
976 vaccinees/patients collected at / during D0, D7 / week 1, D21 / weeks 2&3, D28 / week 4, D42 /  
977 weeks 5&6, and D90 /  $\geq$ week 7 after vaccination / COVID-19 symptom onset (x-axis). The color  
978 scale encodes the median values of log<sub>10</sub> MSD AU/mL concentrations.

979 (B) Box-whisker plots show the development of antibody responses in longitudinal samples from  
980 vaccinees / patients collected at / during D0, D7 / week 1, D21 / weeks 2&3, D28 / week 4, D42 /  
981 weeks 5&6, and D90 /  $\geq$ week 7 after vaccination / COVID-19 symptom onset (x-axis). Box-  
982 whisker plots show the interquartile range as the box and the whisker ends as the most extreme  
983 values within 1.5 times the interquartile range below the 25% quantile and above the 75% quantile.

984 Statistical test: pairwise Wilcoxon rank sum test with Bonferroni correction. \* $p < 0.05$ , \*\* $p < 0.01$ ,  
985 \*\*\* $p < 0.001$ .

986 Individuals were classified as vaccinees who have not been previously exposed to SARS-CoV-2  
987 (Vaccinees); outpatients (Outpt) and hospital admitted patients (Admit); intensive care unit (ICU)  
988 patients, and those who died from their illness (Death).

989 (C) Box-whisker plots show anti-SARS-CoV-1 spike and anti-HCoV spike antibody responses in  
990 plasma samples from individuals who received BNT162b2 prime (D0, n = 59 individuals), second  
991 dose (D21, n = 58 individuals) and third dose (around month 9, n = 36 individuals) vaccination.  
992 Box-whisker plots show the interquartile range as the box and the whisker ends as the most extreme  
993 values within 1.5 times the interquartile range below the 25% quantile and above the 75% quantile.

994  
995 **Figure S4: Greater breadth of IgG binding to SARS-CoV-2 variant RBDs following**  
996 **BNT162b2 vaccination compared to infection with Wuhan-Hu-1 SARS-CoV-2 (Validation**  
997 **cohort), related to Figure 3.**

998 (A, B) Anti-SARS-CoV-2 Wuhan-Hu-1 and viral variant RBD IgG responses are shown for  
999 Stanford individuals who received BNT162b2 vaccination and for Wuhan-Hu-1-infected COVID-  
1000 19 Stanford patient cohort 2 at different time points after vaccination / COVID-19 symptom onset.  
1001 Box-whisker plots show the interquartile range as the box and the whisker ends as the most extreme  
1002 values within 1.5 times the interquartile range below the 25% quantile and above the 75% quantile.  
1003 Significance between groups were tested with pairwise Wilcoxon rank sum test with Bonferroni  
1004 correction. \* $p < 0.05$ , \*\* $p < 0.01$ , \*\*\* $p < 0.001$ .

1005 (A) Anti-RBD IgG concentrations.

1006 (B) Ratios of anti-Wuhan-Hu-1 to variant RBD IgG concentration.

1007 (C) Anti-SARS-CoV-2 Wuhan-Hu-1 and viral variant spike IgG responses as anti-spike IgG  
1008 concentrations (upper panels) and as ratios of anti-Wuhan-Hu-1 to variant spike IgG concentration  
1009 (lower panels) are shown for Stanford individuals who received BNT162b2 vaccination and for  
1010 Wuhan-Hu-1-infected COVID-19 Stanford patient cohort 1 and 2 samples. Box-whisker plots  
1011 show the interquartile range as the box and the whisker ends as the most extreme values within 1.5

1012 times the interquartile range below the 25% quantile and above the 75% quantile. Significance  
1013 between groups were tested with pairwise Wilcoxon rank sum test with Bonferroni correction.  
1014 \* $p < 0.05$ , \*\* $p < 0.01$ , \*\*\* $p < 0.001$ .

1015 (D) Percentage blocking of ACE2 binding to RBD of specified viral variants by plasma  
1016 antibodies of BNT162b2 vaccinees and Stanford patient cohort 2 samples.

1017

1018 **Figure S5: Anti-SARS-CoV-2 RBD IgG signatures following BNT162b2 vaccination and**  
1019 **SARS-CoV-2 infection, related to Figure 5.**

1020 (A) Ratios of anti-Wuhan-Hu-1 to variant RBD IgG concentration are shown for Stanford  
1021 individuals who received BNT162b2 vaccination at different time points after second dose (D21,  
1022  $n = 58$  individuals) and third dose (around month 9,  $n = 36$  individuals) vaccination. Box-whisker  
1023 plots show the interquartile range as the box and the whisker ends as the most extreme values  
1024 within 1.5 times the interquartile range below the 25% quantile and above the 75% quantile.

1025 (B) Principal component analysis (PCA) of anti-SARS-CoV-2 Wuhan-Hu-1 and viral variant RBD  
1026 IgG concentrations across Stanford BNT162b2 vaccinees, Stanford COVID-19 patient cohort 2  
1027 and SARS-CoV-2 variant-infected patients.

1028

1029 **Figure S6: Disrupted LN GCs in COVID-19 patients versus mRNA vaccinees, related to**  
1030 **Figure 6.**

1031 (A) LN GC histology for COVID-19 patients (left) and mRNA vaccinees (right) evaluated with 4-  
1032 color Co-detection by indexing (CODEX) immunofluorescence analysis for CD20 (red), CD3  
1033 (blue), BCL6 (magenta) and CD21 (yellow) markers of B cells, T cells, GC B cells (or T follicular  
1034 helper cells) and follicular dendritic cells, respectively.

1035 (B) Representative CD21 immunohistochemistry of secondary (left) and primary (right) follicles  
1036 of four autopsy patients who died of COVID-19 and two control autopsy patients.  
1037

Journal Pre-proof

1038 **References**

- 1039 Arevalo, C.P., Sage, V.L., Bolton, M.J., Eilola, T., Jones, J.E., Kormuth, K.A., Nturibi, E.,  
 1040 Balmaseda, A., Gordon, A., Lakdawala, S.S., et al. (2020). Original antigenic sin priming of  
 1041 influenza virus hemagglutinin stalk antibodies. *PNAS* *117*, 17221–17227.
- 1042 Arunachalam, P.S., Scott, M.K.D., Hagan, T., Li, C., Feng, Y., Wimmers, F., Grigoryan, L.,  
 1043 Trisal, M., Edara, V.V., Lai, L., et al. (2021). Systems vaccinology of the BNT162b2 mRNA  
 1044 vaccine in humans. *Nature* *596*, 410–416.
- 1045 Baden, L.R., El Sahly, H.M., Essink, B., Kotloff, K., Frey, S., Novak, R., Diemert, D., Spector,  
 1046 S.A., Rouphael, N., Creech, C.B., et al. (2021). Efficacy and Safety of the mRNA-1273 SARS-  
 1047 CoV-2 Vaccine. *New England Journal of Medicine* *384*, 403–416.
- 1048 Bankhead, P., Loughrey, M.B., Fernández, J.A., Dombrowski, Y., McArt, D.G., Dunne, P.D.,  
 1049 McQuaid, S., Gray, R.T., Murray, L.J., Coleman, H.G., et al. (2017). QuPath: Open source  
 1050 software for digital pathology image analysis. *Sci Rep* *7*, 16878.
- 1051 Beach, T.G., Adler, C.H., Sue, L.I., Serrano, G., Shill, H.A., Walker, D.G., Lue, L., Roher, A.E.,  
 1052 Dugger, B.N., Maarouf, C., et al. (2015). Arizona Study of Aging and Neurodegenerative  
 1053 Disorders and Brain and Body Donation Program. *Neuropathology* *35*, 354–389.
- 1054 Black, S., Phillips, D., Hickey, J.W., Kennedy-Darling, J., Venkataraman, V.G., Samusik, N.,  
 1055 Goltsev, Y., Schürch, C.M., and Nolan, G.P. (2021). CODEX multiplexed tissue imaging with  
 1056 DNA-conjugated antibodies. *Nat Protoc* *16*, 3802–3835.
- 1057 Bollinger, R.C., Kline, R.L., Francis, H.L., Moss, M.W., Bartlett, J.G., and Quinn, T.C. (1992).  
 1058 Acid Dissociation Increases the Sensitivity of p24 Antigen Detection for the Evaluation of  
 1059 Antiviral Therapy and Disease Progression in Asymptomatic Human Immunodeficiency Virus-  
 1060 Infected Persons. *The Journal of Infectious Diseases* *165*, 913–916.
- 1061 Choi, A., Koch, M., Wu, K., Chu, L., Ma, L., Hill, A., Nunna, N., Huang, W., Oestreicher, J.,  
 1062 Colpitts, T., et al. (2021). Safety and immunogenicity of SARS-CoV-2 variant mRNA vaccine  
 1063 boosters in healthy adults: an interim analysis. *Nat Med* *27*, 2025–2031.
- 1064 Chu, L., Montefiori, D., Huang, W., Nestorova, B., Chang, Y., Carfi, A., Edwards, D.K.,  
 1065 Oestreicher, J., Legault, H., Girard, B., et al. (2021). Immune Memory Response After a Booster  
 1066 Injection of mRNA-1273 for Severe Acute Respiratory Syndrome Coronavirus-2 (SARS-CoV-  
 1067 2). *MedRxiv* 2021.09.29.21264089.
- 1068 Cirelli, K.M., Carnathan, D.G., Nogal, B., Martin, J.T., Rodriguez, O.L., Upadhyay, A.A.,  
 1069 Enemuo, C.A., Gebru, E.H., Choe, Y., Viviano, F., et al. (2019). Slow Delivery Immunization  
 1070 Enhances HIV Neutralizing Antibody and Germinal Center Responses via Modulation of  
 1071 Immunodominance. *Cell* *177*, 1153-1171.e28.
- 1072 Cloutier, J.M., Allard, G., Bean, G.R., Hornick, J.L., and Charville, G.W. (2021). PDGFB RNA  
 1073 in situ hybridization for the diagnosis of dermatofibrosarcoma protuberans. *Mod Pathol* *34*,  
 1074 1521–1529.

- 1075 Corman, V.M., Landt, O., Kaiser, M., Molenkamp, R., Meijer, A., Chu, D.K., Bleicker, T.,  
1076 Brünink, S., Schneider, J., Schmidt, M.L., et al. (2020). Detection of 2019 novel coronavirus  
1077 (2019-nCoV) by real-time RT-PCR. *Euro Surveill* 25, 2000045.
- 1078 Dashdorj, N.J., Wirz, O.F., Röltgen, K., Haraguchi, E., Buzzanco, A.S., Sibai, M., Wang, H.,  
1079 Miller, J.A., Solis, D., Sahoo, M.K., et al. (2021a). Direct comparison of antibody responses to  
1080 four SARS-CoV-2 vaccines in Mongolia. *Cell Host Microbe* 29, 1738-1743.e4.
- 1081 Dashdorj, N.J., Dashdorj, N.D., Mishra, M., Danzig, L., Briese, T., Lipkin, W.I., and Mishra, N.  
1082 (2021b). Molecular and serological investigation of the 2021 COVID-19 case surge in  
1083 Mongolian vaccinees. *MedRxiv* 2021.08.11.21261915.
- 1084 Earle, K.A., Ambrosino, D.M., Fiore-Gartland, A., Goldblatt, D., Gilbert, P.B., Siber, G.R., Dull,  
1085 P., and Plotkin, S.A. (2021). Evidence for antibody as a protective correlate for COVID-19  
1086 vaccines. *Vaccine* 39, 4423–4428.
- 1087 Elsner, R.A., and Shlomchik, M.J. (2020). Germinal Center and Extrafollicular B Cell Responses  
1088 in Vaccination, Immunity, and Autoimmunity. *Immunity* 53, 1136–1150.
- 1089 Falsey, A.R., Frenck, R.W., Walsh, E.E., Kitchin, N., Absalon, J., Gurtman, A., Lockhart, S.,  
1090 Bailey, R., Swanson, K.A., Xu, X., et al. (2021). SARS-CoV-2 Neutralization with BNT162b2  
1091 Vaccine Dose 3. *New England Journal of Medicine* 385, 1627–1629.
- 1092 Feng, S., Phillips, D.J., White, T., Sayal, H., Aley, P.K., Bibi, S., Dold, C., Fuskova, M., Gilbert,  
1093 S.C., Hirsch, I., et al. (2021). Correlates of protection against symptomatic and asymptomatic  
1094 SARS-CoV-2 infection. *Nat Med* 27, 2032–2040.
- 1095 Feng, Z., Diao, B., Wang, R., Wang, G., Wang, C., Tan, Y., Liu, L., Wang, C., Liu, Y., Liu, Y.,  
1096 et al. (2020). The Novel Severe Acute Respiratory Syndrome Coronavirus 2 (SARS-CoV-2)  
1097 Directly Decimates Human Spleens and Lymph Nodes. *MedRxiv* 2020.03.27.20045427.
- 1098 Garcia-Beltran, W.F., Denis, K.J.S., Hoelzemer, A., Lam, E.C., Nitido, A.D., Sheehan, M.L.,  
1099 Berrios, C., Ofoman, O., Chang, C.C., Hauser, B.M., et al. (2021). mRNA-based COVID-19  
1100 vaccine boosters induce neutralizing immunity against SARS-CoV-2 Omicron variant. *Cell* 0.
- 1101 Gilbert, P.B., Montefiori, D.C., McDermott, A.B., Fong, Y., Benkeser, D., Deng, W., Zhou, H.,  
1102 Houchens, C.R., Martins, K., Jayashankar, L., et al. (2022). Immune correlates analysis of the  
1103 mRNA-1273 COVID-19 vaccine efficacy clinical trial. *Science* 375, 43–50.
- 1104 Goltsev, Y., Samusik, N., Kennedy-Darling, J., Bhate, S., Hale, M., Vazquez, G., Black, S., and  
1105 Nolan, G.P. (2018). Deep Profiling of Mouse Splenic Architecture with CODEX Multiplexed  
1106 Imaging. *Cell* 174, 968-981.e15.
- 1107 Gostic, K.M., Ambrose, M., Worobey, M., and Lloyd-Smith, J.O. (2016). Potent protection  
1108 against H5N1 and H7N9 influenza via childhood hemagglutinin imprinting. *Science* 354, 722–  
1109 726.

- 1110 Greaney, A.J., Loes, A.N., Crawford, K.H.D., Starr, T.N., Malone, K.D., Chu, H.Y., and Bloom,  
1111 J.D. (2021a). Comprehensive mapping of mutations in the SARS-CoV-2 receptor-binding  
1112 domain that affect recognition by polyclonal human plasma antibodies. *Cell Host & Microbe* 29,  
1113 463-476.e6.
- 1114 Greaney, A.J., Loes, A.N., Gentles, L.E., Crawford, K.H.D., Starr, T.N., Malone, K.D., Chu,  
1115 H.Y., and Bloom, J.D. (2021b). Antibodies elicited by mRNA-1273 vaccination bind more  
1116 broadly to the receptor binding domain than do those from SARS-CoV-2 infection. *Sci Transl*  
1117 *Med* 13, eabi9915.
- 1118 Harvey, W.T., Carabelli, A.M., Jackson, B., Gupta, R.K., Thomson, E.C., Harrison, E.M.,  
1119 Ludden, C., Reeve, R., Rambaut, A., Peacock, S.J., et al. (2021). SARS-CoV-2 variants, spike  
1120 mutations and immune escape. *Nat Rev Microbiol* 19, 409–424.
- 1121 Haslbauer, J.D., Matter, M.S., Stalder, A.K., and Tzankov, A. (2021). Histomorphological  
1122 patterns of regional lymph nodes in COVID-19 lungs. *Pathologe* 1–9.
- 1123 Havenar-Daughton, C., Newton, I.G., Zare, S.Y., Reiss, S.M., Schwan, B., Suh, M.J., Hasteh, F.,  
1124 Levi, G., and Crotty, S. (2020). Normal human lymph node T follicular helper cells and germinal  
1125 center B cells accessed via fine needle aspirations. *Journal of Immunological Methods* 479,  
1126 112746.
- 1127 Hoffmann, M., Krüger, N., Schulz, S., Cossmann, A., Rocha, C., Kempf, A., Nehlmeier, I.,  
1128 Graichen, L., Moldenhauer, A.-S., Winkler, M.S., et al. (2021). The Omicron variant is highly  
1129 resistant against antibody-mediated neutralization – implications for control of the COVID-19  
1130 pandemic. *Cell* 0.
- 1131 Hogan, C.A., Sahoo, M.K., Huang, C., Garamani, N., Stevens, B., Zehnder, J., and Pinsky, B.A.  
1132 (2020). Comparison of the Panther Fusion and a laboratory-developed test targeting the envelope  
1133 gene for detection of SARS-CoV-2. *J Clin Virol* 127, 104383.
- 1134 Israel, A., Shenhar, Y., Green, I., Merzon, E., Golan-Cohen, A., Schäffer, A.A., Ruppin, E.,  
1135 Vinker, S., and Magen, E. (2021). Large-scale study of antibody titer decay following  
1136 BNT162b2 mRNA vaccine or SARS-CoV-2 infection. *MedRxiv* 2021.08.19.21262111.
- 1137 Kaneko, N., Kuo, H.-H., Boucau, J., Farmer, J.R., Allard-Chamard, H., Mahajan, V.S.,  
1138 Piechocka-Trocha, A., Lefteri, K., Osborn, M., Bals, J., et al. (2020). Loss of Bcl-6-Expressing T  
1139 Follicular Helper Cells and Germinal Centers in COVID-19. *Cell* 183, 143-157.e13.
- 1140 Keehner, J., Horton, L.E., Binkin, N.J., Laurent, L.C., Pride, D., Longhurst, C.A., Abeles, S.R.,  
1141 and Torriani, F.J. (2021). Resurgence of SARS-CoV-2 Infection in a Highly Vaccinated Health  
1142 System Workforce. *N Engl J Med* 385, 1330–1332.
- 1143 Khoury, D.S., Cromer, D., Reynaldi, A., Schlub, T.E., Wheatley, A.K., Juno, J.A., Subbarao, K.,  
1144 Kent, S.J., Triccas, J.A., and Davenport, M.P. (2021). Neutralizing antibody levels are highly  
1145 predictive of immune protection from symptomatic SARS-CoV-2 infection. *Nat Med* 27, 1205–  
1146 1211.

- 1147 Lam, J.H., Smith, F.L., and Baumgarth, N. (2020). B Cell Activation and Response Regulation  
1148 During Viral Infections. *Viral Immunol* 33, 294–306.
- 1149 Lederer, K., Castaño, D., Gómez Atria, D., Oguin, T.H., Wang, S., Manzoni, T.B., Muramatsu,  
1150 H., Hogan, M.J., Amanat, F., Cherubin, P., et al. (2020). SARS-CoV-2 mRNA Vaccines Foster  
1151 Potent Antigen-Specific Germinal Center Responses Associated with Neutralizing Antibody  
1152 Generation. *Immunity* 53, 1281-1295.e5.
- 1153 Lederer, K., Parvathaneni, K., Painter, M.M., Bettini, E., Agarwal, D., Lundgreen, K.A.,  
1154 Weirick, M., Goel, R.R., Xu, X., Drapeau, E.M., et al. (2021). Germinal center responses to  
1155 SARS-CoV-2 mRNA vaccines in healthy and immunocompromised individuals. *MedRxiv*  
1156 2021.09.16.21263686.
- 1157 Levin, E.G., Lustig, Y., Cohen, C., Fluss, R., Indenbaum, V., Amit, S., Doolman, R., Asraf, K.,  
1158 Mendelson, E., Ziv, A., et al. (2021). Waning Immune Humoral Response to BNT162b2 Covid-  
1159 19 Vaccine over 6 Months. *N Engl J Med* NEJMoa2114583.
- 1160 Lima, M. da R.Q., Nogueira, R.M.R., Filippis, A.M.B. de, Nunes, P.C.G., Sousa, C.S. de, Silva,  
1161 M.H. da, and Santos, F.B. dos (2014). A simple heat dissociation method increases significantly  
1162 the ELISA detection sensitivity of the nonstructural-1 glycoprotein in patients infected with  
1163 DENV type-4. *Journal of Virological Methods* 204, 105–108.
- 1164 Lindgren, G., Ols, S., Liang, F., Thompson, E.A., Lin, A., Hellgren, F., Bahl, K., John, S.,  
1165 Yuzhakov, O., Hassett, K.J., et al. (2017). Induction of Robust B Cell Responses after Influenza  
1166 mRNA Vaccination Is Accompanied by Circulating Hemagglutinin-Specific ICOS+ PD-1+  
1167 CXCR3+ T Follicular Helper Cells. *Front Immunol* 8, 1539.
- 1168 Lindsay, K.E., Bhosle, S.M., Zurla, C., Beyersdorf, J., Rogers, K.A., Vanover, D., Xiao, P.,  
1169 Araínga, M., Shirreff, L.M., Pitard, B., et al. (2019). Visualization of early events in mRNA  
1170 vaccine delivery in non-human primates via PET-CT and near-infrared imaging. *Nat Biomed*  
1171 *Eng* 3, 371–380.
- 1172 Long, Q.-X., Liu, B.-Z., Deng, H.-J., Wu, G.-C., Deng, K., Chen, Y.-K., Liao, P., Qiu, J.-F., Lin,  
1173 Y., Cai, X.-F., et al. (2020). Antibody responses to SARS-CoV-2 in patients with COVID-19.  
1174 *Nat Med* 26, 845–848.
- 1175 Miles, S.A., Balden, E., Magpantay, L., Wei, L., Leiblein, A., Hofheinz, D., Toedter, G., Stiehm,  
1176 E.R., and Bryson, Y. (1993). Rapid Serologic Testing with Immune-Complex-Dissociated HIV  
1177 p24 Antigen for Early Detection of HIV Infection in Neonates. *New England Journal of*  
1178 *Medicine* 328, 297–302.
- 1179 Ogata, A.F., Maley, A.M., Wu, C., Gilboa, T., Norman, M., Lazarovits, R., Mao, C.-P., Newton,  
1180 G., Chang, M., Nguyen, K., et al. (2020). Ultra-Sensitive Serial Profiling of SARS-CoV-2  
1181 Antigens and Antibodies in Plasma to Understand Disease Progression in COVID-19 Patients  
1182 with Severe Disease. *Clinical Chemistry* 66, 1562–1572.

- 1183 Pardi, N., Hogan, M.J., Naradikian, M.S., Parkhouse, K., Cain, D.W., Jones, L., Moody, M.A.,  
1184 Verkerke, H.P., Myles, A., Willis, E., et al. (2018). Nucleoside-modified mRNA vaccines induce  
1185 potent T follicular helper and germinal center B cell responses. *J Exp Med* 215, 1571–1588.
- 1186 Plante, J.A., Mitchell, B.M., Plante, K.S., Debbink, K., Weaver, S.C., and Menachery, V.D.  
1187 (2021). The variant gambit: COVID-19's next move. *Cell Host & Microbe* 29, 508–515.
- 1188 Polack, F.P., Thomas, S.J., Kitchin, N., Absalon, J., Gurtman, A., Lockhart, S., Perez, J.L., Pérez  
1189 Marc, G., Moreira, E.D., Zerbini, C., et al. (2020). Safety and Efficacy of the BNT162b2 mRNA  
1190 Covid-19 Vaccine. *New England Journal of Medicine* 383, 2603–2615.
- 1191 Röltgen, K., and Boyd, S.D. (2021). Antibody and B cell responses to SARS-CoV-2 infection  
1192 and vaccination. *Cell Host Microbe* 29, 1063–1075.
- 1193 Röltgen, K., Powell, A.E., Wirz, O.F., Stevens, B.A., Hogan, C.A., Najeeb, J., Hunter, M.,  
1194 Wang, H., Sahoo, M.K., Huang, C., et al. (2020). Defining the features and duration of antibody  
1195 responses to SARS-CoV-2 infection associated with disease severity and outcome. *Sci Immunol*  
1196 5, eabe0240.
- 1197 Sadoff, J., Gray, G., Vandebosch, A., Cárdenas, V., Shukarev, G., Grinsztejn, B., Goepfert, P.A.,  
1198 Truyers, C., Fennema, H., Spiessens, B., et al. (2021). Safety and Efficacy of Single-Dose  
1199 Ad26.COVS.2.S Vaccine against Covid-19. *New England Journal of Medicine* 384, 2187–2201.
- 1200 Schürch, C.M., Bhate, S.S., Barlow, G.L., Phillips, D.J., Noti, L., Zlobec, I., Chu, P., Black, S.,  
1201 Demeter, J., McIlwain, D.R., et al. (2020). Coordinated Cellular Neighborhoods Orchestrate  
1202 Antitumoral Immunity at the Colorectal Cancer Invasive Front. *Cell* 182, 1341-1359.e19.
- 1203 Turner, J.S., O'Halloran, J.A., Kalaidina, E., Kim, W., Schmitz, A.J., Zhou, J.Q., Lei, T., Thapa,  
1204 M., Chen, R.E., Case, J.B., et al. (2021). SARS-CoV-2 mRNA vaccines induce persistent human  
1205 germinal centre responses. *Nature* 596, 109–113.
- 1206 Voysey, M., Clemens, S.A.C., Madhi, S.A., Weckx, L.Y., Folegatti, P.M., Aley, P.K., Angus, B.,  
1207 Baillie, V.L., Barnabas, S.L., Bhorat, Q.E., et al. (2021). Safety and efficacy of the ChAdOx1  
1208 nCoV-19 vaccine (AZD1222) against SARS-CoV-2: an interim analysis of four randomised  
1209 controlled trials in Brazil, South Africa, and the UK. *The Lancet* 397, 99–111.
- 1210 Walsh, E.E., Frenck, R.W., Falsey, A.R., Kitchin, N., Absalon, J., Gurtman, A., Lockhart, S.,  
1211 Neuzil, K., Mulligan, M.J., Bailey, R., et al. (2020). Safety and Immunogenicity of Two RNA-  
1212 Based Covid-19 Vaccine Candidates. *New England Journal of Medicine* 383, 2439–2450.
- 1213 Wang, H., Miller, J.A., Verghese, M., Sibai, M., Solis, D., Mfuh, K.O., Jiang, B., Iwai, N., Mar,  
1214 M., Huang, C., et al. (2021). Multiplex SARS-CoV-2 Genotyping Reverse Transcriptase PCR for  
1215 Population-Level Variant Screening and Epidemiologic Surveillance. *J Clin Microbiol* 59,  
1216 e0085921.
- 1217 Wheatley, A.K., Fox, A., Tan, H.-X., Juno, J.A., Davenport, M.P., Subbarao, K., and Kent, S.J.  
1218 (2021). Immune imprinting and SARS-CoV-2 vaccine design. *Trends Immunol* 42, 956–959.

- 1219 Woodruff, M.C., Ramonell, R.P., Nguyen, D.C., Cashman, K.S., Saini, A.S., Haddad, N.S., Ley,  
1220 A.M., Kyu, S., Howell, J.C., Ozturk, T., et al. (2020). Extrafollicular B cell responses correlate  
1221 with neutralizing antibodies and morbidity in COVID-19. *Nature Immunology* 21, 1506–1516.
- 1222 Wu, K., Choi, A., Koch, M., Ma, L., Hill, A., Nunna, N., Huang, W., Oestreicher, J., Colpitts, T.,  
1223 Bennett, H., et al. (2021). Preliminary Analysis of Safety and Immunogenicity of a SARS-CoV-2  
1224 Variant Vaccine Booster. *MedRxiv* 2021.05.05.21256716.
- 1225 Yuan, M., Liu, H., Wu, N.C., and Wilson, I.A. (2021). Recognition of the SARS-CoV-2 receptor  
1226 binding domain by neutralizing antibodies. *Biochemical and Biophysical Research*  
1227 *Communications* 538, 192–203.
- 1228 Zhang, A., Stacey, H.D., Mullarkey, C.E., and Miller, M.S. (2019). Original Antigenic Sin: How  
1229 First Exposure Shapes Lifelong Anti-Influenza Virus Immune Responses. *The Journal of*  
1230 *Immunology* 202, 335–340.
- 1231

## Highlights

- Vaccination confers broader IgG binding of variant RBDs than SARS-CoV-2 infection
- Imprinting from initial antigen exposures alters IgG responses to viral variants
- Histology of mRNA vaccinee lymph nodes shows abundant germinal centers
- Vaccine spike antigen and mRNA persist for weeks in lymph node germinal centers

## In Brief

Human antibody responses to SARS-CoV-2 differ between vaccination and infection, with vaccination (regardless of vaccine type) inducing more productive lymph node germinal center responses and a broader range of IgG neutralizing antibodies capable of recognizing viral variants.

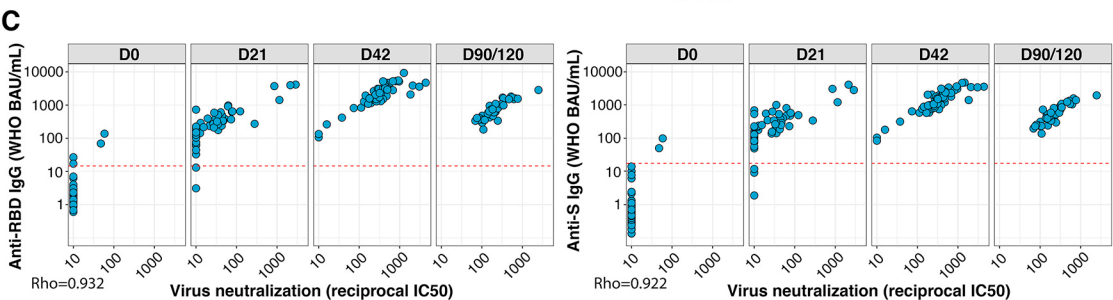
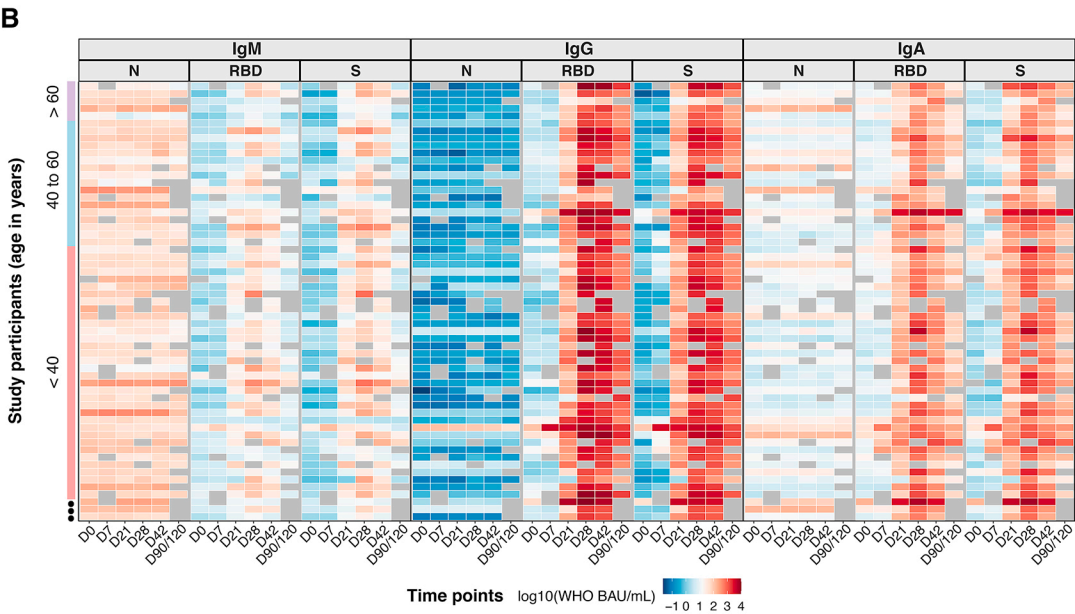
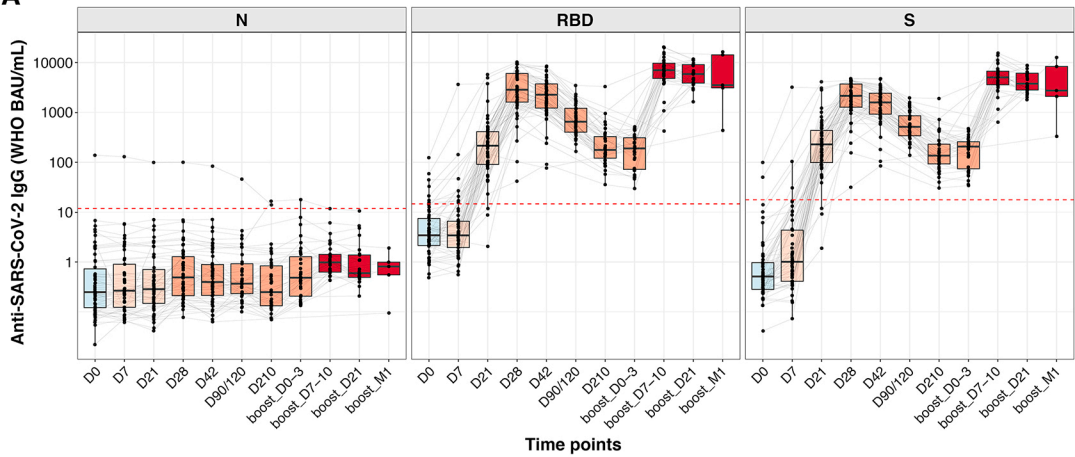
## KEY RESOURCES TABLE

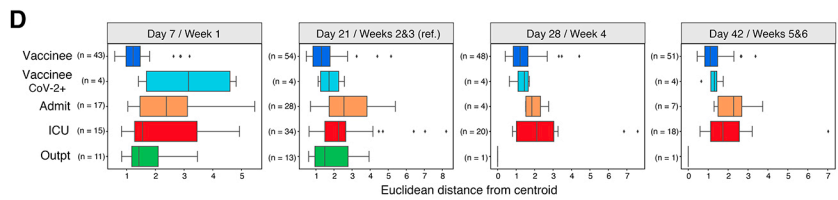
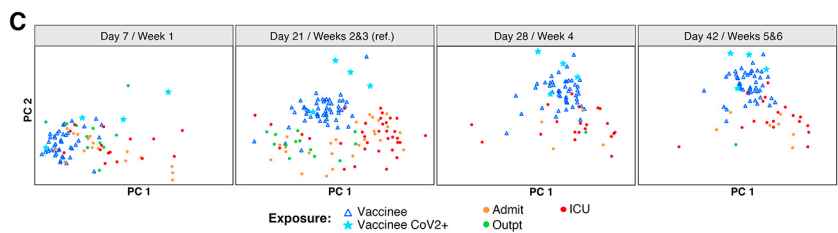
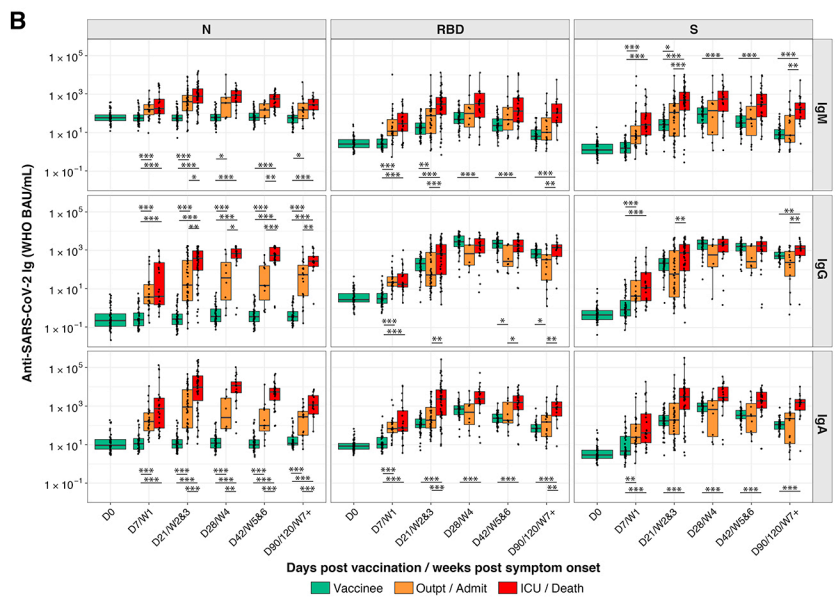
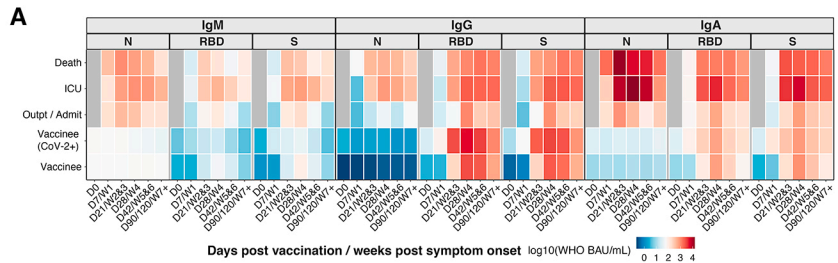
## Key resources table

REAGENT or RESOURCE	SOURCE	IDENTIFIER
<b>Antibodies</b>		
Sulfo-tag conjugated anti-human IgG	Meso Scale Discovery	Cat#D21ADF-3
Sulfo-tag conjugated anti-human IgM	Meso Scale Discovery	Cat#D21ADD-3
Sulfo-tag conjugated anti-human IgA	Meso Scale Discovery	Cat#D21ADE-3
ACE2 calibration reagent	Meso Scale Discovery	Cat#C01ADG-2
Reference Standard 1	Meso Scale Discovery	Cat#C00ADK-2
Anti-CD20 (clone SP32), for CODEX	Abcam	Cat#ab236434
Anti-CD3 (clone EP449E), for CODEX	Akoya Biosciences	Cat#4450027
Anti-CD21 (clone EP3093), for CODEX	Akoya Biosciences	Cat#4450027
Anti-BCL6 (clone IG191E/A8), for CODEX	Biolegend	Cat#648301
Anti-CD20 (clone L26), for IHC	Dako	Cat#M0755
Anti-CD3 (clone 2GV6), for IHC	Ventana	Cat#790-4341
Anti-CD21 (clone EP3093), for IHC	Ventana	Cat#760-4438
Anti-BCL6 (clone GL191E/A8), for IHC	Ventana	Cat#760-4241
Anti-PD-1 (clone NAT105), for IHC	Cell-Marque	Cat#315M-96
Anti-CovNP T62 (polyclonal)	Sino Biological	Cat#40143-T62
Anti-SARS-CoV-2 spike (clone 1A9)	GeneTex	Cat#GTX632604
<b>Biological samples</b>		
Plasma and saliva samples from 59 individuals vaccinated with BNT162b2 vaccine	This paper	N/A
Plasma samples from 196 individuals vaccinated with BNT162b2, ChAdOx1-S, Gam-COVID-Vac, BBIBP-CorV vaccines	ND Dashdorj, Ulaanbaatar, Mongolia	<a href="http://www.onomfoundation.org">http://www.onomfoundation.org</a>
Plasma samples from 188 patients infected with SARS-CoV-2	This paper	N/A
Plasma samples from 50 individuals infected with SARS-CoV-2 variants	This paper	N/A
37 plasma and 20 saliva samples from healthy human control individuals	Sean N. Parker Center for Allergy & Asthma Research	<a href="https://med.stanford.edu/allergyandasthma.html">https://med.stanford.edu/allergyandasthma.html</a>
Six post-mortem peribronchial lymph nodes from patients who died of COVID-19	Banner Health	<a href="https://www.bannerhealth.com/">https://www.bannerhealth.com/</a>
Three post-mortem peribronchial lymph nodes from pre-pandemic control patients	Banner Health	<a href="https://www.bannerhealth.com/">https://www.bannerhealth.com/</a>
Seven axillary lymph node core needle biopsies from individuals vaccinated with BNT162b2 or mRNA-1273	This paper	N/A
Three axillary lymph node core needle biopsies from unvaccinated individuals	This paper	N/A
<b>Chemicals, peptides, and recombinant proteins</b>		
Sulfo-tag conjugated human ACE2 protein	Meso Scale Discovery	Cat#D21ADG-3
MSD GOLD Read Buffer B	Meso Scale Discovery	Cat#R60AM-2
RNAscope Probe-V-nCoV2019-S	Advanced cell diagnostics	Cat#848561

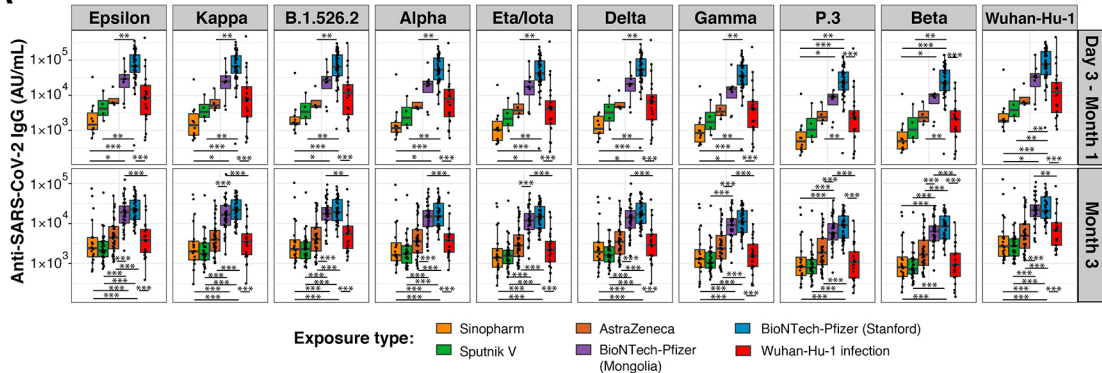
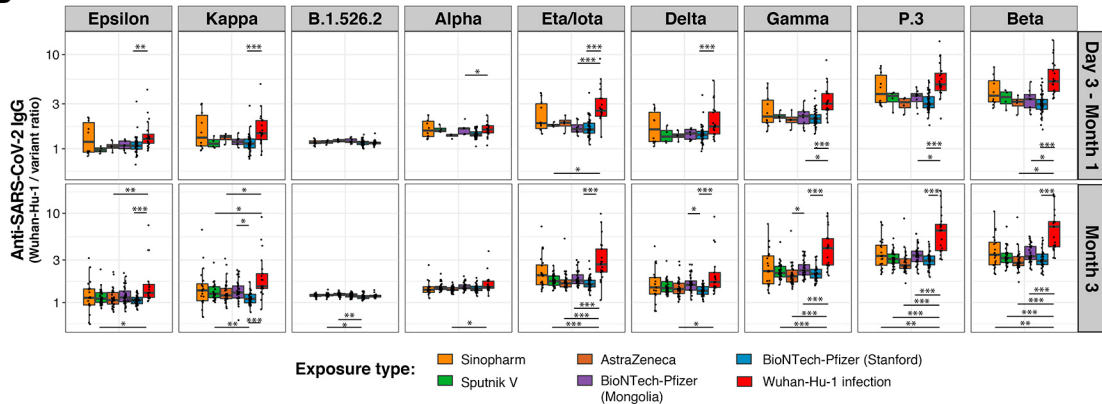
RNAscope Probe S-encoding-mRNA-1273-C1 (targeting 101-1488 of Spike-encoding_contig_assembled_from_Moderna_mRNA-1273_vaccine)	Advanced cell diagnostics	Cat#1104251-C1
RNAscope Probe S-encoding-BNT-162b2-C1 (targeting 101-1143 of Figure1_032321_Spike-encoding_contig_assembled_from_BioNTech/Pfizer_BNT-162b2_vaccine)	Advanced cell diagnostics	Cat#1104241-C1
RNA ISH Positive Control Probe PPIB	Advanced cell diagnostics	Cat#RS7755
SARS-CoV-2 Spike protein	ATUM, custom	N/A
Bond Aspirating Probe Cleaning Solution	Leica Microsystems	Cat#CS9100
Bond Dewax Solution	Leica Microsystems	Cat#AR9222
Bond Epitope Retrieval 2	Leica Microsystems	Cat#AR9640
Bond Epitope Retrieval 1	Leica Microsystems	Cat#AR9961
Bond Enzyme Pre-treatment Kit	Leica Microsystems	Cat#AR9551
Bond Mixing Stations	Leica Microsystems	Cat#S21.1971
Bond Open Containers, 30mL	Leica Microsystems	Cat#OP309700
Bond Open Containers, 7mL	Leica Microsystems	Cat#OP79193
Bond Polymer Refine Kit	Leica Microsystems	Cat#DS9800
Bond Primary Antibody Diluent	Leica Microsystems	Cat#AR9352
Bond Slide Labs and Ribbon	Leica Microsystems	Cat#S21.4564
Bond Titration Kit	Leica Microsystems	Cat#OPT9049
Bond Titration Container	Leica Microsystems	Cat#OTP9719
Bond Universal Covertiles	Leica Microsystems	Cat#S21.4611
Bond Wash Solution	Leica Microsystems	Cat#AR9590
Hematoxylin II	Ventana	Cat#790-2208
Bluing, 760-2037EZ Prep Solution (10X)	Ventana	Cat#950-102
OptiView Detection Kit	Ventana	Cat#760-700
Protease 1	Ventana	Cat#760-2018
Protease 2	Ventana	Cat#760-2019
Reaction Buffer (10X)	Ventana	Cat#950-300
SSC Solution	Ventana	Cat#950-110
Ultra CC1 Solution	Ventana	Cat#950-224
Ultra LCS Solution	Ventana	Cat#650-210
UltraView Universal DAB Detection Kit	Ventana	Cat#760-500
Vantage Clear Overlay	Ventana	Cat#1749400
Dako Target Retrieval at pH9	Aligent	Cat#S2368
Hydrogen Peroxide 30% (diluted to 3%)	Thermo-Fisher	Cat#H325500
Normal Horse Serum 2.5%	Victor Labs	Cat#S-2012
ImmPress HRP Universal Secondary Antibody	Victor Labs	Cat#MP-7500
Dako Liquid DAB+ Substrate Chromogen System	Aligent	Cat#K3468
<b>Critical commercial assays</b>		
V-PLEX Coronavirus Panel 2 (IgG) Kit	Meso Scale Discovery	Cat#K15369U
V-PLEX Coronavirus Panel 2 (IgM) Kit	Meso Scale Discovery	Cat#K15370U
V-PLEX Coronavirus Panel 2 (IgA) Kit	Meso Scale Discovery	Cat#K15371U
V-PLEX SARS-CoV-2 Panel 9 (IgG) Kit	Meso Scale Discovery	Cat#K15448U
V-PLEX SARS-CoV-2 Panel 11 (IgG) Kit	Meso Scale Discovery	Cat#K15455U
V-PLEX SARS-CoV-2 Panel 11 (ACE2) Kit	Meso Scale Discovery	Cat#K15458U

V-PLEX SARS-CoV-2 Panel 20 (IgG) Kit	Meso Scale Discovery	Cat#K15551U
S-PLEX SARS-CoV-2 Spike Kit	Meso Scale Discovery	Cat#K150ADJS
RNAScope 2.5 HD Assay-RED kit	Advanced cell diagnostics	Cat#322350
<b>Deposited data</b>		
Electrochemiluminescence data	This paper; Mendeley Data	DOI:10.17632/hy3zm69f57.1
Original code	This paper; Github	<a href="https://github.com/boyd-lab/covid-infection-vs-vaccination">https://github.com/boyd-lab/covid-infection-vs-vaccination</a>
Original code	This paper; Zenodo	<a href="https://doi.org/10.5281/zenodo.5854880">https://doi.org/10.5281/zenodo.5854880</a>
Virus neutralization antibody data from individuals vaccinated with BNT162b2	Arunachalam et al., 2021	DOI:10.1038/s41586-021-03791-x
<b>Software and algorithms</b>		
R version 4.0.5 base packages	The R Foundation	<a href="https://www.rstudio.com/products/rstudio/download/">https://www.rstudio.com/products/rstudio/download/</a>
R version 4.0.5 ggplot2 package	The R Foundation	<a href="https://cran.r-project.org/web/packages/ggplot2/index.html">https://cran.r-project.org/web/packages/ggplot2/index.html</a>
QuPath version 0.2.3	Bankhead, P. et al.	PMID: 29203879 <a href="https://qupath.github.io/">https://qupath.github.io/</a>
Python version 3.7.10	Python Software Foundation	<a href="https://www.python.org">https://www.python.org</a>
CODEX® MAV	Akoya Biosciences	<a href="https://help.codex.bio">https://help.codex.bio</a>

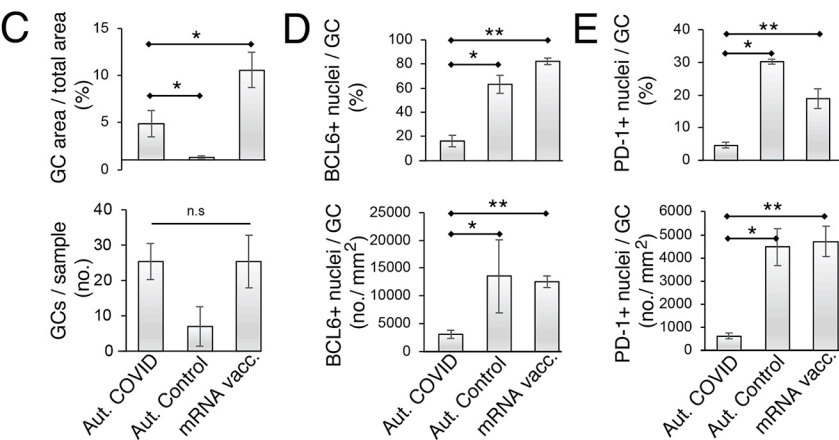
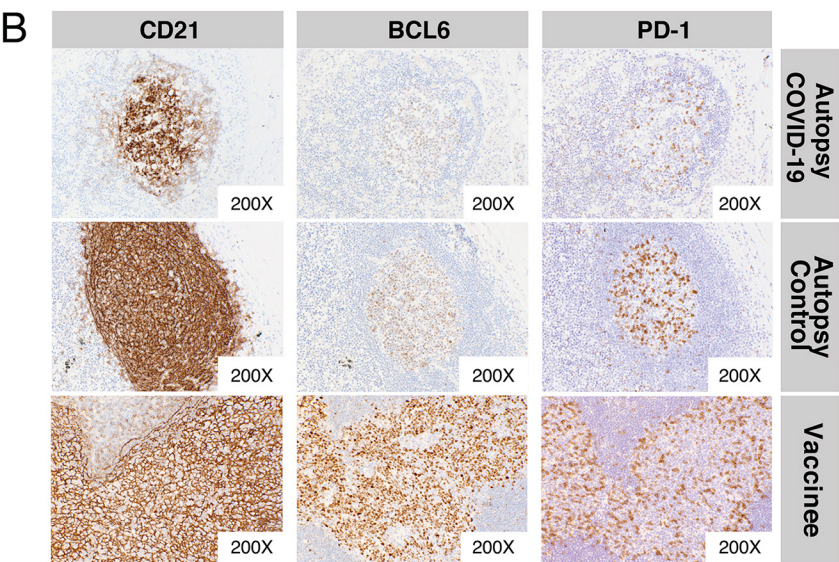
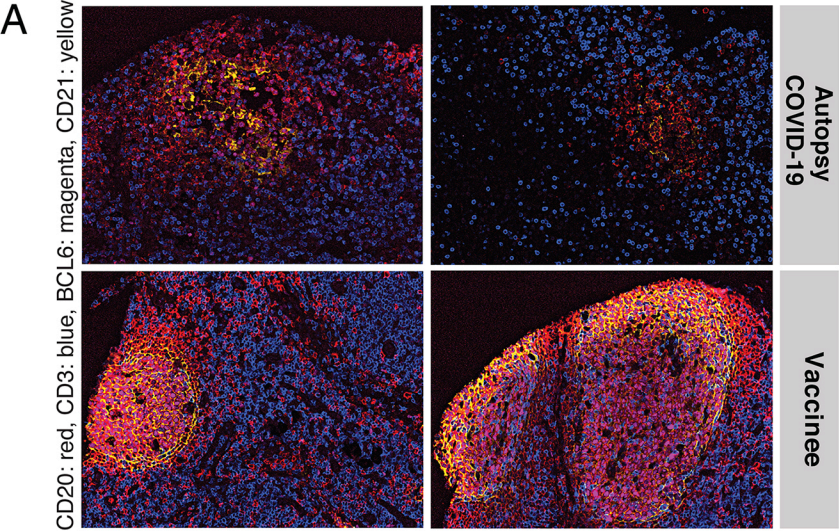


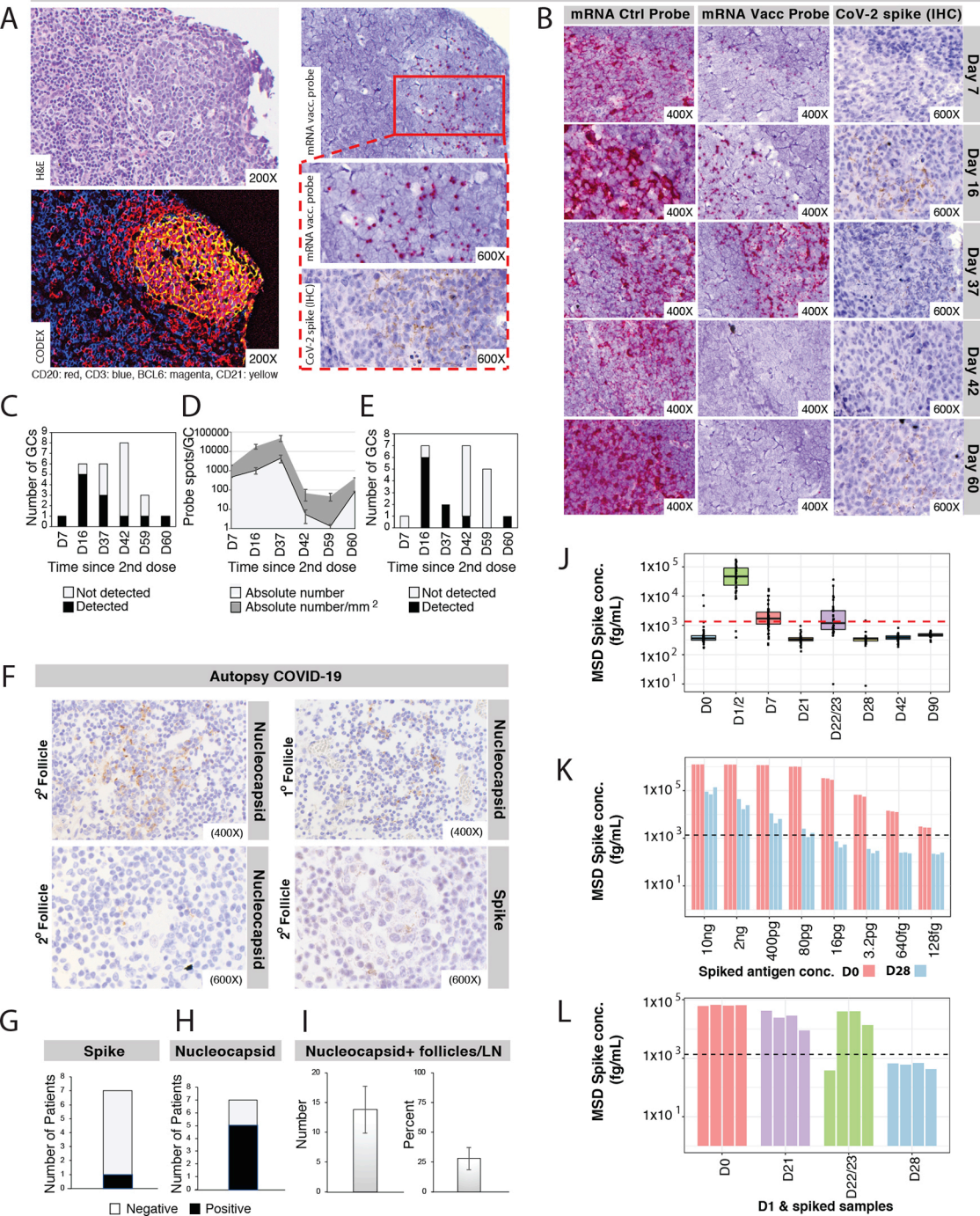


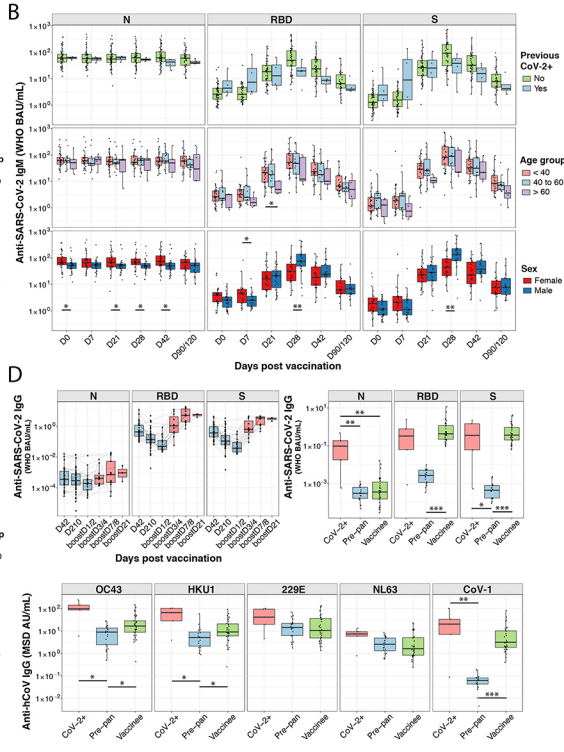
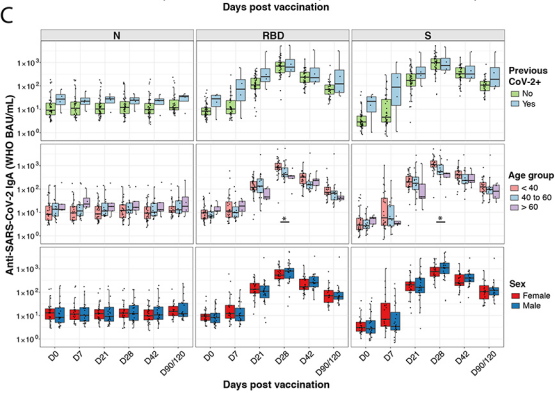
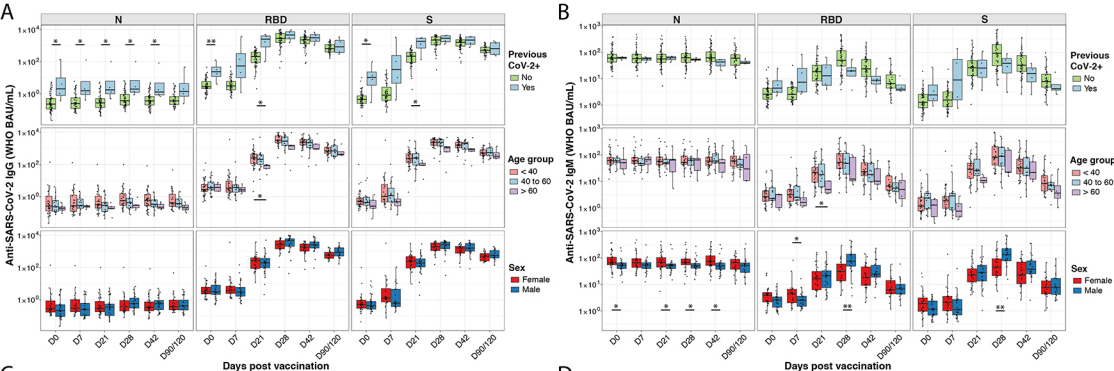


**A****B**

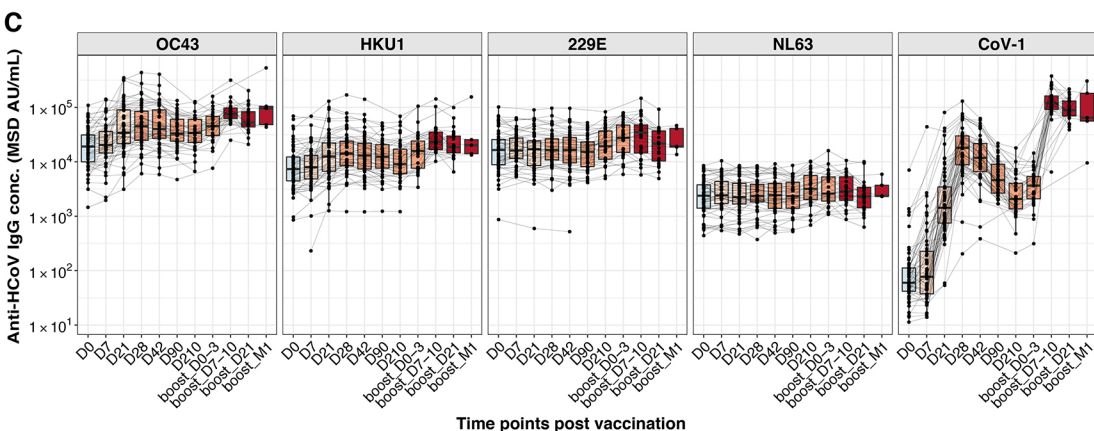
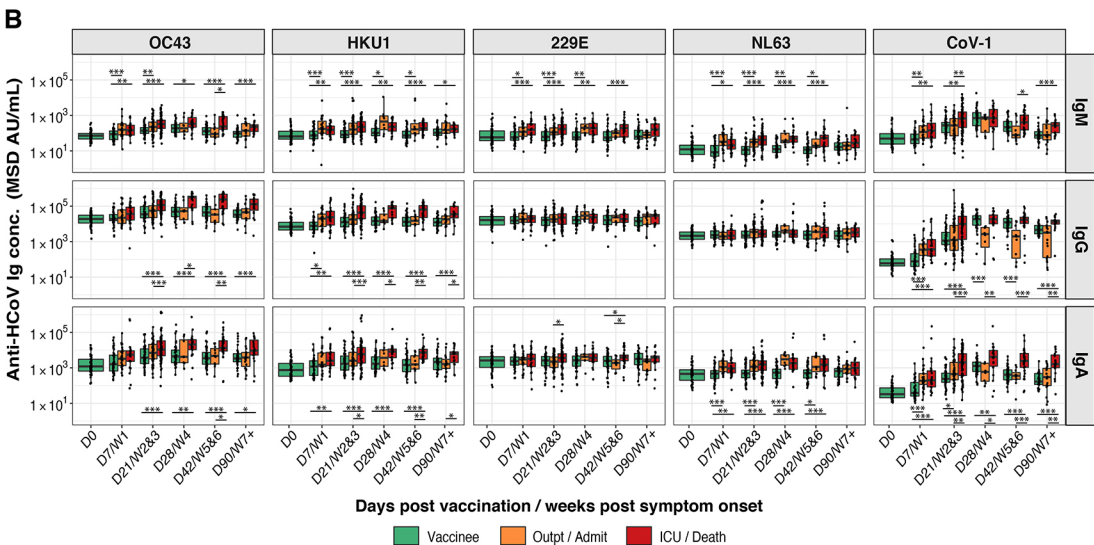
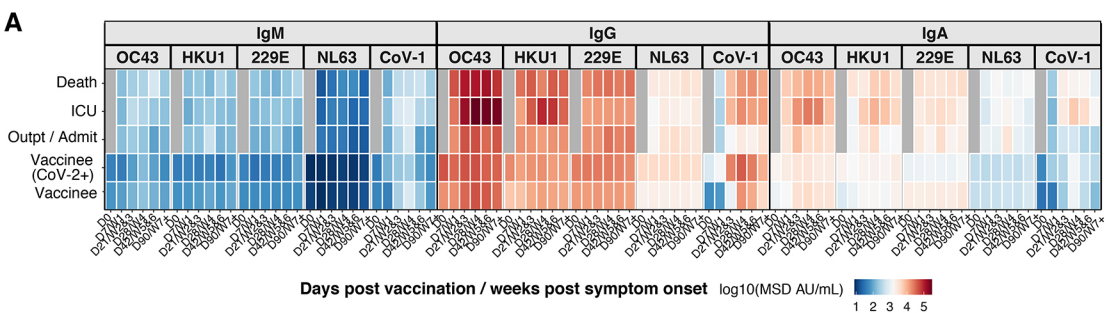


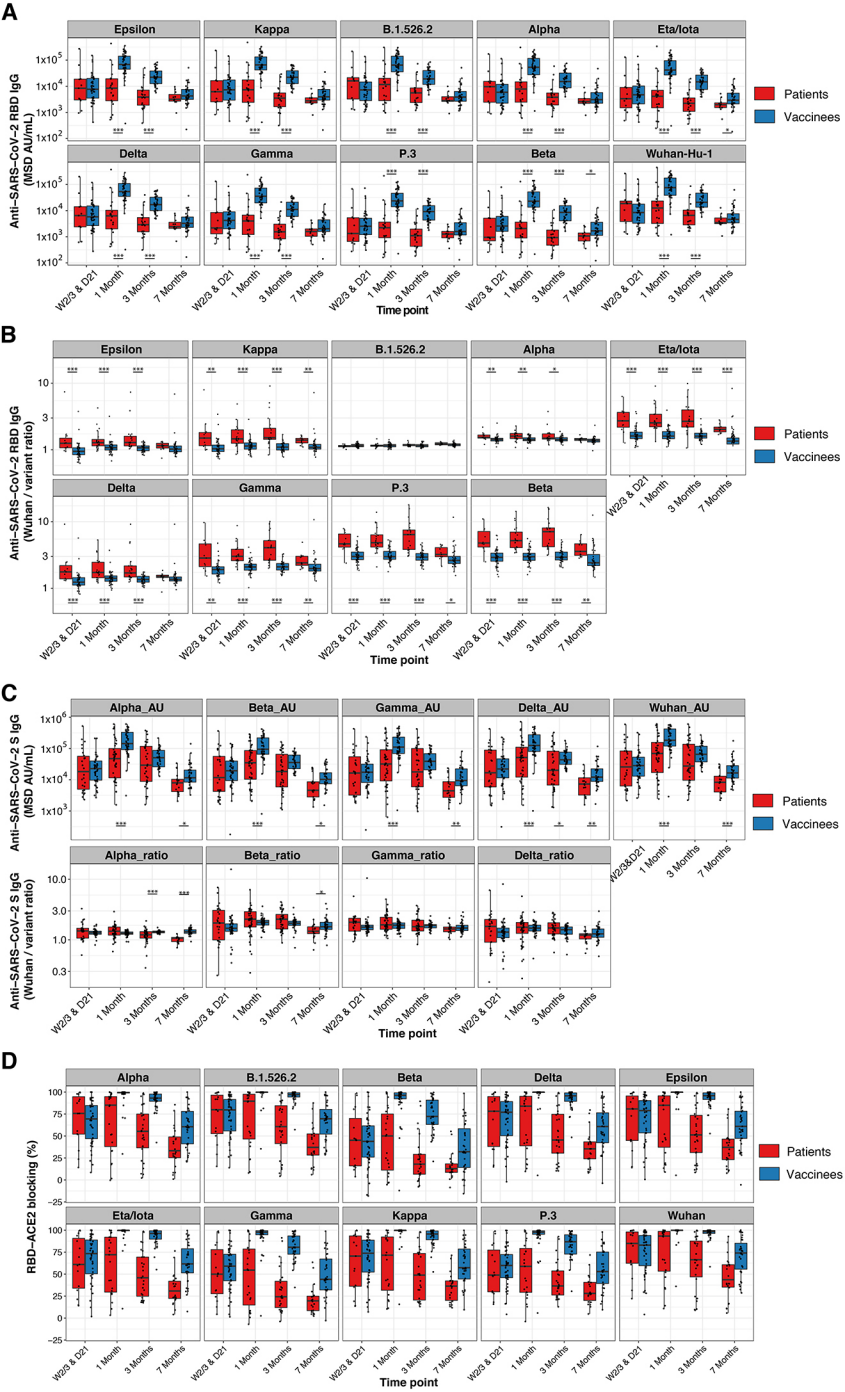


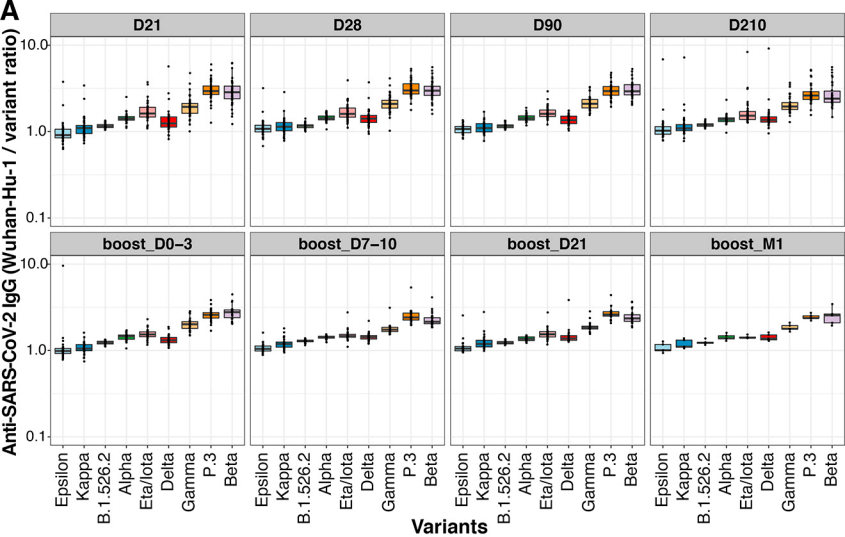












**B**

